

Gene Transfer with AAV9-PHP.B Rescues Hearing in a Mouse Model of Usher Syndrome 3A and Transduces Hair Cells in a Non-human Primate

Bence György,^{1,2,8} Elise J. Meijer,^{1,8} Maryna V. Ivanchenko,^{1,8} Kelly Tenneson,³ Frederick Emond,³ Killian S. Hanlon,^{1,2} Artur A. Indzhukulian,^{1,4} Adrienn Volak,² K. Domenica Karavitaki,¹ Panos I. Tamvakologos,¹ Mark Vezina,³ Vladimir K. Berezovskii,¹ Richard T. Born,¹ Maureen O'Brien,⁵ Jean-François Lafond,³ Yvan Arsenijevic,⁶ Margaret A. Kenna,⁷ Casey A. Maguire,² and David P. Corey¹

¹Department of Neurobiology, Harvard Medical School, Boston, MA 02115, USA; ²Molecular Neurogenetics Unit, Massachusetts General Hospital, Harvard Medical School, Charlestown, MA 02114, USA; ³Charles River Laboratories, Senneville, QC, Canada; ⁴Department of Otolaryngology, Massachusetts Eye and Ear, Harvard Medical School, Boston, MA 02114, USA; ⁵Charles River Laboratories, Frederick, MD 21701, USA; ⁶Unit of Retinal Degeneration and Regeneration, Department of Ophthalmology, University of Lausanne, Jules-Gonin Eye Hospital, Lausanne, Switzerland; ⁷Department of Otolaryngology, Boston Children's Hospital, Harvard Medical School, Boston, MA 02115, USA

Hereditary hearing loss often results from mutation of genes expressed by cochlear hair cells. Gene addition using AAV vectors has shown some efficacy in mouse models, but clinical application requires two additional advances. First, new AAV capsids must mediate efficient transgene expression in both inner and outer hair cells of the cochlea. Second, to have the best chance of clinical translation, these new vectors must also transduce hair cells in non-human primates. Here, we show that an AAV9 capsid variant, PHP.B, produces efficient transgene expression of a GFP reporter in both inner and outer hair cells of neonatal mice. We show also that AAV9-PHP.B mediates almost complete transduction of inner and outer HCs in a non-human primate. In a mouse model of Usher syndrome type 3A deafness (gene *CLRN1*), we use AAV9-PHP.B encoding *Clnr1* to partially rescue hearing. Thus, we have identified a vector with promise for clinical treatment of hereditary hearing disorders, and we demonstrate, for the first time, viral transduction of the inner ear of a primate with an AAV vector.

INTRODUCTION

Hearing loss occurs in approximately 1/1,000 births, with roughly half having a genetic cause. The disease burden is substantial and lifelong. Many of the deafness genes identified affect hair cells (HCs), the sensory cells of the inner ear, so a promising strategy to treat hereditary deafness is gene delivery to HCs with viral vectors. Adeno-associated virus (AAV) serotype 1 vector has been used for viral transduction of HCs; however, it only transduces inner HCs (IHCs) and not the equally important outer HCs (OHCs).^{1,2} Studies using AAV8 have shown variable results transducing OHCs via round window membrane (RWM) injection.^{3,4}

Recently, our group and others demonstrated efficient gene delivery to IHCs and OHCs in neonatal mice, using new AAV-based sys-

tems.⁵⁻⁷ Both represent significant advances over conventional AAV1. However, significant challenges remain for clinical translation of AAV-based gene therapy for deafness. First, gene transfer to the cochlea has been performed almost exclusively in neonatal mice, with no reports in non-human primates (NHPs), so the translational potential of various AAVs for cochlear gene therapy in humans is unknown. Second, in many human hereditary deafnesses, the HCs are thought to degenerate during development, so postnatal gene therapy interventions might have no target.⁸ Thus, many studies showing rescue of hearing in neonatal mice in models of human deafness do not necessarily apply to humans.

To address these issues, we first sought a gene delivery vector for effective gene therapy to all cochlear HCs, in several relevant species. We used GFP expression to assess the efficacy of a recently described AAV9 capsid variant, AAV9-PHP.B, which was originally selected for transduction of central neurons after systemic delivery in mice.⁹ AAV9-PHP.B mediated efficient transgene expression in the IHCs and OHCs of neonatal mice and rats and produced transgene expression in many cochlear cell types in juvenile macaque, including HCs.

As a model, we selected the recessive deafness and blindness disorder Usher syndrome type 3A (Usher 3A; caused by mutations in *CLRN1*). In Usher 3A, the hearing loss is not profound at birth but is

Received 13 November 2018; accepted 14 November 2018;
<https://doi.org/10.1016/j.omtm.2018.11.003>.

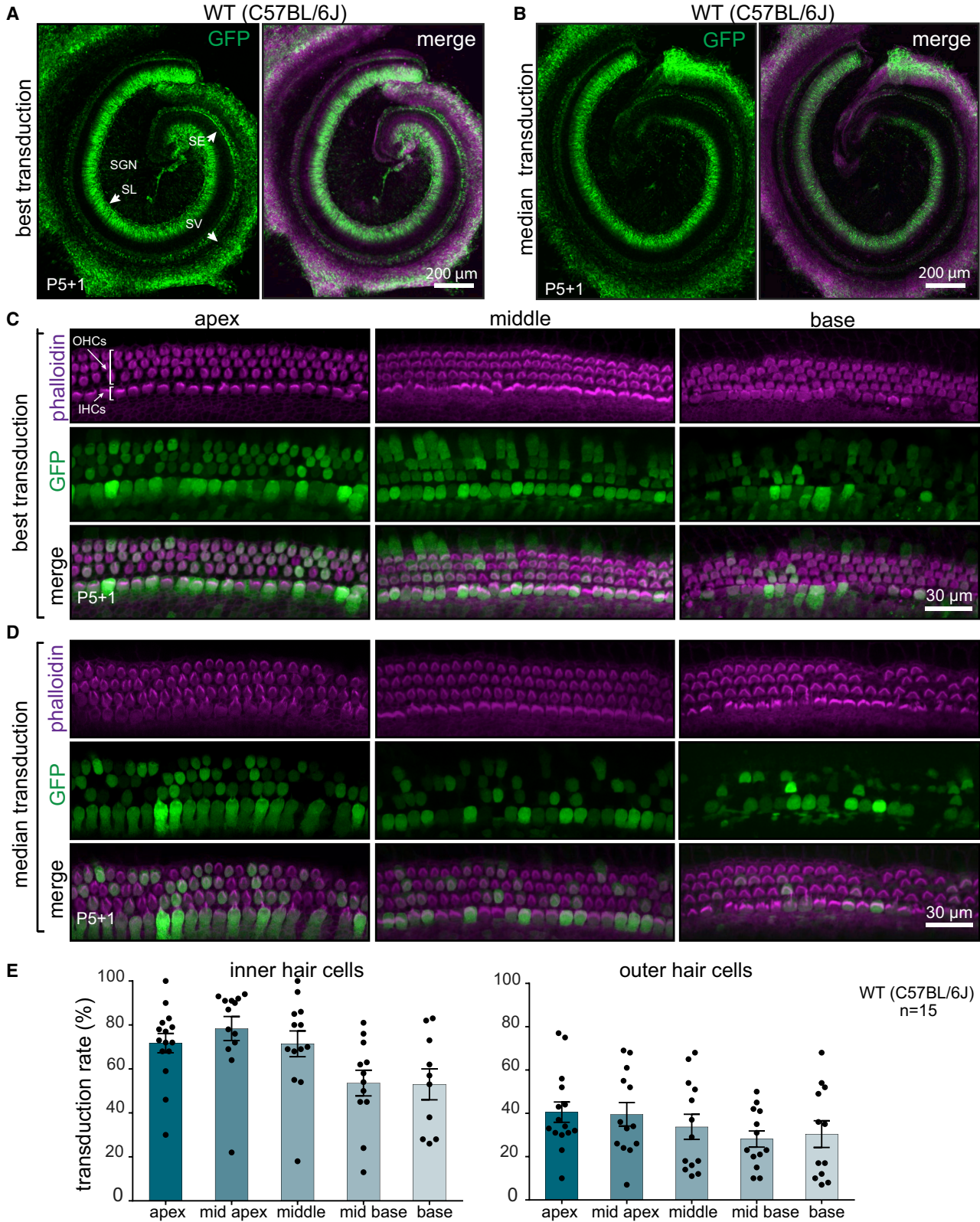
⁸These authors contributed equally to this work.

Correspondence: Casey A. Maguire, Molecular Neurogenetics Unit, Massachusetts General Hospital, 149 13th Street, Charlestown, MA 02129, USA.
E-mail: cmaguire@mgh.harvard.edu

Correspondence: David P. Corey, Department of Neurobiology, Harvard Medical School, 220 Longwood Avenue, Boston, MA 02115, USA.

E-mail: dcorey@hms.harvard.edu





(legend on next page)

progressive, providing a reasonable window for AAV-mediated gene therapy intervention. We used AAV9-PHP.B to deliver a normal copy of the *Cln1* coding sequence to cochleas in a mouse model of Usher 3A and found significant rescue of hearing. Together, these data support a feasible path toward clinical development of a gene therapy for hereditary hearing loss.

RESULTS

AAV9-PHP.B Efficiently Transduces Hair Cells in Neonatal Mice

First, we tested the transduction efficiency of AAV9-PHP.B capsid using a single-stranded (ss) AAV transgene expression cassette, with a GFP reporter driven by the chicken beta actin (CBA) promoter. The scalae tympani of the cochleas of neonatal C57BL/6 mice were injected via the RWM at postnatal day 1 (P1) with 5×10^{10} vector genomes (VGs) of AAV9-PHP.B-CBA-GFP. Five days later, mice were sacrificed, and cochlear explants were cultured for one additional day before fixation and GFP expression analysis. We observed robust transduction in the spiral ganglion region, sensory epithelium, and lateral wall of the cochlea (Figures 1A and 1B; Figure S1). Higher magnification images of the sensory epithelium revealed efficient GFP expression in both IHCs and OHCs (Figures 1C and 1D) but not in the supporting cells surrounding the HCs. Transduction efficiency was 60%–80% for IHCs and 30%–40% for OHCs, depending on the location (Figure 1E; Figure S2). For OHCs, there was a significant gradient of transduction from apex to base, with more efficient transduction in the apex (linear regression, $R^2 = 0.83$, $p = 0.029$), but for IHCs, there was no statistically significant gradient.

In one animal (out of five), we observed vector transduction of a few cells in the uninjected contralateral ear (Figure S3). It is possible that some vector diffused through cerebrospinal fluid to the other ear in a neonatal animal.

We also injected adult (4-week-old C57BL/6) mice with 2×10^{10} VGs of AAV9-PHP.B-CBA-GFP through the posterior semicircular canal. Although almost all IHCs from apex to base were transduced, no OHC transduction was observed (Figures S4A and S4B), suggesting that, in mice, AAV9-PHP.B can transduce OHCs only in neonates (at least for the tested delivery routes). We observed robust transduction of the vestibular system (Figure S4C).

Hordeaux et al. recently found that the enhanced transduction of CNS neurons in C57BL/6 mice by systemically administered AAV9-PHP.B did not translate to the BALB/cJ mouse strain,¹⁰ so we asked whether AAV9-PHP.B efficacy in the neonatal C57BL/6 mouse cochlea would

extend to neonatal CD1 mouse cochlea. Injection of AAV9-PHP.B-GFP into P1 CD1 mice resulted in robust GFP expression in both IHCs and OHCs in the cochlea (Figures 2A and 2B). We observed 60%–80% transduction of IHCs and 40%–70% transduction of OHCs (Figure 2C). There was significantly higher transduction efficiency in CD1 animals compared to that in C57BL/6 animals (Figure 2D) (Mann-Whitney test, $p < 0.04$ for IHCs, and $p < 0.004$ for OHCs; data are from all regions analyzed).

Finally, we asked whether efficacy translates to another rodent species, Sprague-Dawley rats. We injected two P1 neonatal pups via the RWM at a dose of 1.2×10^{10} VGs. As in neonatal mice, we observed GFP-positive cells in the regions of spiral ganglion, sensory epithelium, and lateral wall. The transduction efficiency was higher in one of the injected rats (Figures S5A and S5B); higher magnification of the sensory epithelium in that animal revealed robust IHC and OHC transduction (Figure S5A).

Taken together, these results confirm that the AAV9-PHP.B capsid is an efficient vector to target neonatal sensory HCs in two strains of mice as well as in rats.

Cln1 Expression in the Murine Inner Ear

To test AAV9-PHP.B in an animal model of hereditary deafness, we first selected a deafness gene for which postnatal treatment is feasible in human. In Usher 3A (caused by mutations in *CLRN1*), the hearing loss is not profound at birth but is progressive, providing a reasonable window for AAV-mediated gene therapy. We first investigated normal *Cln1* expression in the developing inner ear. The Shared Harvard Inner-Ear Laboratory Database (SHIELD¹¹) revealed highly enriched expression of *Cln1* in cochlear and vestibular HCs relative to non-HCs (Figure S6A). Alternative splice forms of *Cln1* have been identified, so we separately dissected organs of Corti and spiral ganglion regions from embryonic day (E)17 up to P7 in CD1 mice and performed RT-PCR with primers in exon 1 and exon 4. RT-PCR analysis revealed that isoform 2 of *Cln1* (containing exons 1, 3, and 4) was the predominant mRNA species expressed at all ages (Figure S7); however, isoform 3 (containing exons 1 and 4) was also expressed. Based on the predicted tertiary structure of clarin 1 (Figure S6B) and the fact that the *CLRN1* sequence is highly conserved between species (Figure S6C), we anticipate that isoform 3 would not be functional, as it would lack a conserved transmembrane domain. Isoform 2 was found to be predominant in the retina as well.¹² For therapeutic application, therefore, we cloned the mouse codon-optimized cDNA of isoform 2 of *Cln1* into the AAV expression cassette.

Figure 1. Transduction Efficiency in C57BL/6J Mice of AAV9-PHP.B-CBA-GFP after Neonatal RWM Injection

(A) Low-magnification images of the cochlea showing the highest transduction level. WT, wild-type. (B) The median transduction ($n = 15$). Animals were injected at P1 with 5×10^{10} vector genomes (VGs), and the cochlea was explanted at P5 and cultured for another day (P5+1). The left panel shows GFP staining only; the right panel shows GFP overlaid with phalloidin staining. SGN, spiral ganglion neurons; SE, sensory epithelium; SV, stria vascularis; SL, spiral limbus. (C) High-magnification images of different regions of the cochlea with the highest transduction. (D) High-magnification images of the cochlea with median transduction. (E) Quantification of transduction efficiency in IHCs (left panel) and OHCs (right). Bars indicate mean \pm SEM. To determine the specified regions, we measured the distance from the apex and used the same value for all cochleas (for details, see Figure S2). Not all the cochleas had a preserved basal region, so there are fewer data points for the base.

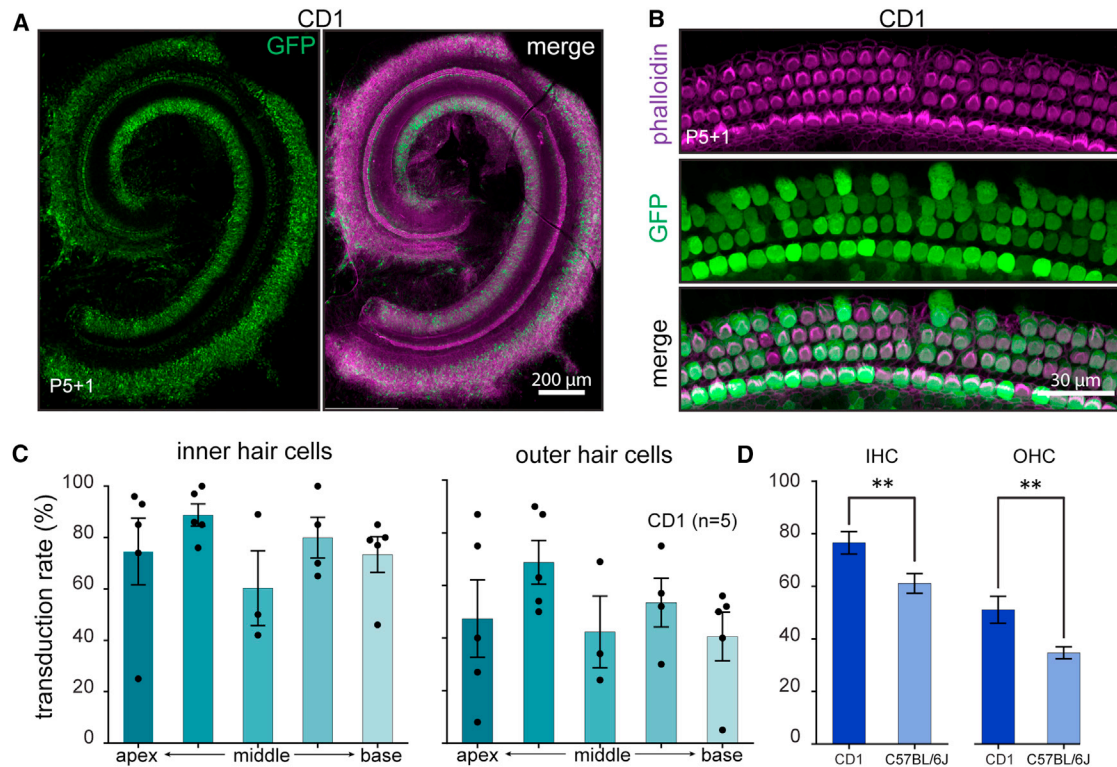


Figure 2. Transduction Efficiency in CD1 Mice of AAV9-PHP.B-CBA-GFP after Neonatal RWM Injection

(A) Low-magnification image of a representative injection in CD1 mouse. Animals ($n = 5$) were injected at P1 with 5×10^{10} VGs, and cochleas were explanted at P5 and cultured for another day (P5+1). Left panel shows GFP staining only; right panel shows GFP overlaid with phalloidin staining. (B) High-magnification image of the sensory epithelium of mid-apex region from the same cochlea as in (A). (C) Quantification of transduction efficiency in IHCs and OHCs. Error bars indicate mean \pm SEM. (D) Transduction efficiency in CD1 compared to C57BL/6J mice (unpaired t test, $p < 0.001$ for IHCs, and $p < 0.009$ for OHCs; data are from all regions analyzed).

Lack of *Clnr1* Leads to Hair Cell Dysfunction

To establish a baseline for rescue, we evaluated the phenotype of *Clnr1*^{-/-}. First, we performed a simple dye loading assay in cochlear explants from heterozygous *Clnr1*^{+/-} or knockout *Clnr1*^{-/-} mice. At P5+1, loading of the styryl dye FM1-43 was significantly decreased in both IHCs and OHCs in knockout mice compared to heterozygotes, indicating impaired mechanotransduction (Figure S8; unpaired t test for all regions combined, $p < 0.0001$ for both IHCs and OHCs) and confirming the results of Geng et al.¹³ Analysis of *Clnr1*^{-/-} hair bundle morphology revealed loss of orientation and disorganization of hair bundles at P5+1, beginning as early as P0+1 (Figure S9).

AAV9-PHP.B-Mediated *Clnr1* Expression in Hair Cells Results in Restoration of Hearing in a Mouse Model of Usher 3A

For AAV-mediated *Clnr1* expression in HCs, we packaged *Clnr1* isoform 2 under the control of the CBA promoter into AAV9-PHP.B (ss genome) with an N-terminal hemagglutinin (HA) tag to allow antibody detection (Figure S10). We observed expression of *Clnr1* mRNA by RT-PCR and of CLRN1 protein by immunostaining, after transfection of the plasmid into 293T cells (Figure S11). Next, we injected 7.4×10^{10} VGs of AAV9-PHP.B-CBA-HA-*Clnr1* into *Clnr1*^{-/-} animals at P1. As expected from previous reports,¹³ we

found robust immunostaining with an anti-HA antibody of *Clnr1* in the hair bundles of IHCs and OHCs. There was staining also in the kinocilium and cuticular plate region (Figures 3A and 3B). Cell bodies showed diffuse immunostaining (Figure 3B). Importantly, transduction efficiency of vector encoding HA-CLRN1 was similar to that seen with vector encoding GFP, with more efficient transduction in the apex compared to that in the base (Figure 3C).

Finally, to test whether we could rescue hearing in *Clnr1*^{-/-} mice with gene addition therapy, we injected P1 cochleas through the RWM with 1.8×10^{11} VGs of untagged AAV9-PHP.B-*Clnr1* ($n = 17$). Uninjected mice ($n = 10$) were used as controls. Four weeks post-injection, an auditory brainstem response (ABR) recording was performed at different frequencies (Figure 3D). Measurement of ABRs in uninjected control *Clnr1*^{-/-} mice ($n = 10$) indicated that they are almost completely deaf by P25, with limited residual hearing in a few animals at 11.3–16 kHz. AAV-injected *Clnr1*^{-/-} mice showed robust hearing rescue at lower frequencies (4–8 kHz); however, there was little or no rescue at the highest frequencies. The absence of rescue at higher frequencies could be related to the relatively low AAV9-PHP.B-mediated CLRN1 expression in the base (Figure 3C). The best hearing restoration was a 50-dB reduction in threshold in two animals at 4

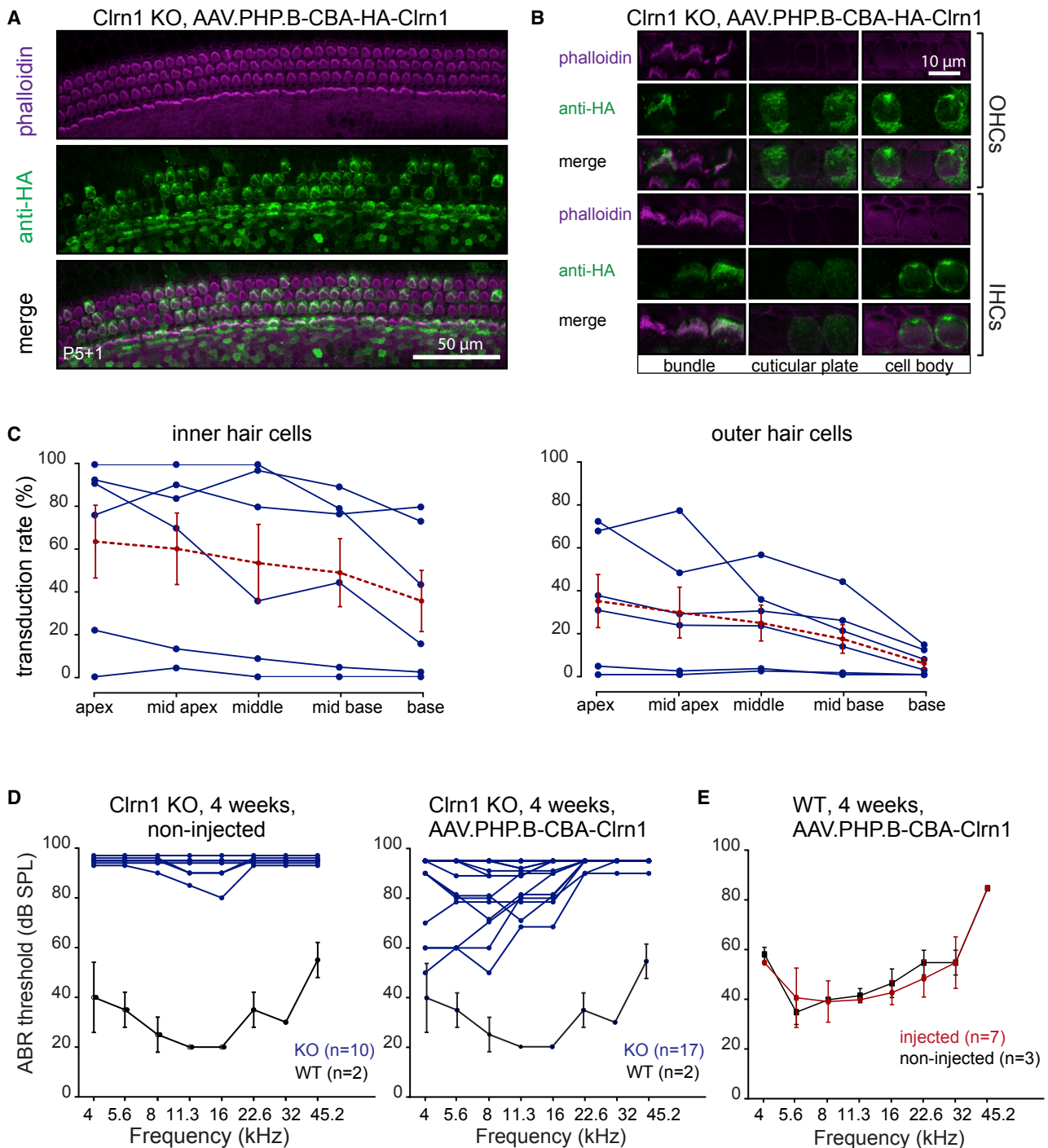


Figure 3. AAV-Mediated Cln1 Delivery Restores Protein Expression in IHCs and OHCs and Rescues Hearing in Cln1 KO Animals

(A) Anti-HA immunostaining of injected C57BL/6J mice. Animals were injected at P1 through the RWM with 7.4×10^{10} VGs of AAV9-PHP.B-CBA-HA-Cln1. Cochleas were explanted at P5 and were cultured for another day (P5+1). Hair bundles were counterstained with phalloidin. (B) Higher magnification images of IHCs and OHCs at different focal planes. Strong fluorescence labeling was observed in the hair bundle region, cuticular plate, and kinocilium. In the cell body, diffuse cytoplasmic staining was detected.

(legend continued on next page)

and 5.6 kHz. Compared to non-injected animals, hearing restoration was significant at 4, 5.6, 8, and 11 kHz (Wilcoxon test, $p < 0.05$ for all indicated frequencies) (Figure S12A). When we compared injected (left) versus non-injected (right) ears, we also observed significantly lower thresholds in injected ears at 4, 5.6, and 8 kHz (Wilcoxon test, $p < 0.05$ for all indicated animals) (Figure S12B).

We also ascertained whether injection of AAV9-PHP.B-*Cln1* would adversely affect the ABR thresholds of normal-hearing mice, a measure of potential vector-related toxicity. P1 wild-type C57BL/6 mice were injected with 4.12×10^{10} VGs of AAV9-PHP.B-*Cln1*, and 4 weeks later, an ABR assay was performed. We observed no distortion of ABR thresholds in injected mice compared to those in untreated mice, suggesting that the surgery and vector expression was well tolerated (Figure 3E).

AAV9-PHP.B Transduces Retinal Cells in Mice

Because Usher 3A patients show late-onset blindness due to retinal degeneration, we tested the ability of AAV9-PHP.B-GFP to transduce retinal cells after subretinal injections (2.1×10^9 VGs) in adult C57BL/6 mice ($n = 6$ retinas injected). With fundus imaging, we observed widespread retinal transduction 8 days post-injection (Figure 4A) in 4 of 6 injected eyes (in 2 eyes, the injections failed). Microscopy revealed robust (~70%–80%) photoreceptor transduction at the injection site in AAV9-PHP.B-GFP-injected eyes (Figure 4B), along with some GFP-positive cells in the inner nuclear layer (INL) and ganglion cell layer (GCL). Results from the other three eyes with successful injection are shown in Figure S13. These results suggest that the AAV-PHP.B capsid can be used to target both inner ear HCs and retinal photoreceptors.

AAV9-PHP.B Transduces Cells in NHP Inner Ear after RWM Injection

As a step toward clinical translation to humans, we asked whether IHCs and OHCs can be transduced by AAV9-PHP.B in NHPs. A male juvenile cynomolgus monkey (animal #1002) was injected in one ear via the RWM with a dose of 3×10^{11} VGs of AAV9-PHP.B-GFP in a volume of 10 μ L, using a trans-mastoid approach similar to that reported by Dai et al.¹⁴ The contralateral (left) ear was used as a control. Seven weeks later, the animal was sacrificed, the temporal bone was extracted and decalcified over 3 months, and the cochlea was sectioned for histological analysis (Figure 5A).

H&E examination of the injected and noninjected cochleas indicated little change associated with the surgery and vector injection. We observed small bone fragments in the middle ear, with minimal inflammation and slight fibrous tissue, which is consistent with temporal bone fragments generated during the surgical procedure. Examination of sections of the cochlea in the injected ear revealed mild

hemorrhage, which is expected with this surgical procedure. We detected some inflammatory cells in the noninjected cochlea. The HCs, stria vascularis, and spiral ganglion neurons had normal morphology (Figures S14 and S15).

We then used anti-GFP antibodies to assess GFP expression in both uninjected and injected ears. While no specific staining was observed in the uninjected ear (Figure 5B, bottom, and 5C, top left), we observed robust GFP immunoreactivity throughout the cochlea in the injected ear (Figure 5B, top). GFP appeared in the organ of Corti, spiral ligament, spiral limbus, and stria vascularis, from the base to the apex. Higher magnification revealed GFP expression by HCs in the organ of Corti (Figure 5C). Quantitation of GFP immunoreactive HCs in cochlear turns in serial sections revealed 92% transduction of IHCs and 92% of OHCs. Widespread transduction in the lateral wall was observed as well (Figure 5D). Additionally, GFP expression was detected with lower intensity in the spiral ganglion neurons (Figure 5E).

We subsequently injected both cochleas of a female juvenile macaque (animal #3501) with 1×10^{11} VGs of AAV9-PHP.B-GFP in a volume of 10 μ L. ABR assays were performed before surgery and 8 weeks post-surgery. ABR waveforms were quite similar in the left injected ear pre- and post-surgery, although the right ear showed some elevation in hearing thresholds compared to pre-treatment waveforms (Figure S16). The animal was killed on the day after ABR, and cochleas were processed for histology and immunostaining. H&E examination of the injected cochleas indicated little change associated with the surgery and vector injection (Figures S17 and S18), similar to animal #1002. In contrast to animal #1002, we observed limited transduction in both injected cochleas in animal #3501. The very few GFP-positive cells were mostly Claudius cells in the organ of Corti and a few cells in the lateral wall (Figure S19). No obvious HC transduction was observed in either cochlea in this animal, perhaps because of the lower dose used or perhaps because of a failure of vector injection.

DISCUSSION

Our results demonstrate that the AAV capsid, AAV9-PHP.B, can mediate efficient transduction of both IHCs and OHCs in the cochleas of neonatal mice, neonatal rats, and a juvenile NHP. Determining the translation potential of AAV capsids is important, as there have been reports of species differences in tropism and transduction. For example, while AAV8 vectors have shown high tropism for hepatocytes in mouse models, they appear to have a preference for murine hepatocytes over human hepatocytes in humanized liver models.¹⁵ Similarly, the AAV9-PHP.B capsid was selected for transduction of the CNS, from a randomized heptamer peptide library inserted in the AAV9 capsid, after intravenous injection of the library in mice.⁹

(C) Proportion of inner and outer hair cells with HA-positive bundles. Blue traces indicate individual animals ($n = 6$); dashed red traces indicate mean \pm SEM. (D) Auditory brainstem response (ABR) of mice injected with AAV9-PHP.B-CBA-*Cln1* (tagless, no HA tag, 1.8×10^{11} VGs were injected). An ABR assay was performed at 4 weeks for vector-injected (right panel; $n = 17$) and non-injected (left panel; $n = 10$) animals. In each panel, the ABR from 4-week-old wild-type C57BL/6J animals is indicated for comparison ($n = 2$; mean \pm SD). (E) ABR testing of AAV9-PHP.B-mediated expression of *Clarin1* on hearing in wild-type C57BL/6J mice ($n = 7$; mean \pm SD).

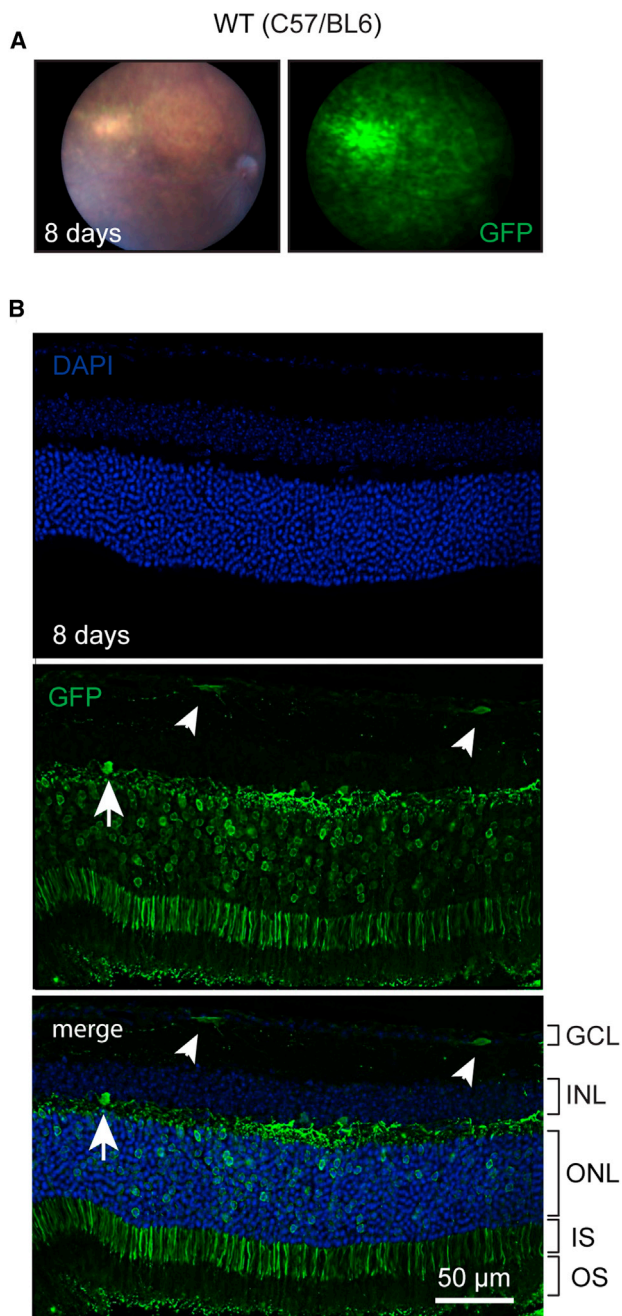


Figure 4. Transduction of Mouse Retina with AAV9-PHP.B-CBA-GFP

Adult (4.5-month-old) C57/BL6 mice were injected subretinally with 2.1×10^9 VG (1 μ L). (A) Many retinal cells were transduced 8 days post-injection. (B) Numerous photoreceptors were GFP positive as well as a few cells in the ganglion cell layer (GCL; small arrowheads) and the inner nuclear layer (INL; large arrowhead). GCL, ganglion cell layer; INL, inner nuclear layer; ONL, outer nuclear layer; IS, inner segment; OS, outer segment.

AAV9-PHP.B is, arguably, the most efficient AAV vector at transduction of mouse neurons and astrocytes after systemic injection to date, with great enhancement over AAV9. However, while the enhance-

ment was confirmed in the mouse strain in which the library was selected, this enhancement was not observed in NHPs.^{10,16}

We first tested PHP.B in the inner ear with the goal of identifying AAV vectors that could mediate efficient transduction as an ss genome, in order to achieve maximum packaging capacity (~ 4.7 kb). We have previously observed that self-complementary (sc) AAV1 vectors are more efficient than ss AAV1 vectors (data not shown), although sc encoding reduces transgene cassette packaging capacity to ~ 2.3 kb. As HCs are not closely related to neurons or astrocytes, we were surprised to see the striking efficiency of the transduction of IHCs and OHCs after local injection of AAV9-PHP.B. This capsid displays a 7-mer peptide, TLAVPFK, between amino acids 588 and 589 (numbering from VP1 protein).⁹ However the mechanism by which AAV9-PHP.B mediates efficient HC transduction is not yet clear.

A number of other AAV variants have been tested for efficacy in the expression of exogenous genes in HCs of neonatal mice. AAV1 was found by both Akil et al.¹ and Askew et al.² to transduce most IHCs, but few OHCs, in neonatal mouse cochlea. For proteins that are primarily expressed only in IHCs, such as the VGLUT3 transporter,¹ AAV1 was adequate for rescue of deafness in a mouse model. However most deafness genes in HCs encode proteins needed in both IHCs and OHCs, so efficient targeting of OHCs is essential. AAV2 and AAV8 were used by Geng et al.,³ with only slightly better results: both transduced IHCs and some OHCs, although the transduction efficiency was not quantified. Dulon et al.¹⁷ also used AAV8 and transduced $\sim 90\%$ of IHCs but only 10% of OHCs. Better results were found with a synthetic AAV, Anc80L65: in the very best cases, nearly 100% of IHCs and OHCs were transduced. With the delivery of $\sim 1.4 \times 10^9$ VGs of Anc80, 30%–60% of IHCs and 10%–60% of OHCs were transduced, whereas there was essentially no transduction by AAV1, AAV2, and AAV8 at the same dose.⁶ For most of these vectors in most studies, efficacy was higher at the low-frequency apex of the cochlea than at the high-frequency base.

AAV9-PHP.B compares favorably to these vectors. At 5×10^{10} VGs with RWM injection of C57BL/6 mice at P0, it transduced 50%–70% of IHCs and up to 100% in the best cases. OHCs were also transduced, at 30%–40% on average and up to 75%. AAV9-PHP.B transduced CD1 mice at even higher rates: $\sim 80\%$ of IHCs and 50% of OHCs.

In adult mice, the transduction profile of HCs differed from that of neonates. Because injection through the RWM in adult mice can damage hearing, delivery can be performed by injection into the posterior semi-circular canal. Vector apparently diffuses easily to the cochlea in mice, because cochlear HCs are readily transduced. With canal injections of $\sim 1 \times 10^9$ VGs of Anc80L65, Suzuki et al.¹⁸ found that nearly all IHCs were transduced and that between 90% (apex) and 20% (base) of the OHCs were transduced. Similarly, a comprehensive comparison of eight AAV variants (AAV1, AAV2, AAV6.2, AAV8, AAV9, rh.39, rh.43, and Anc80L65; $1\text{--}2 \times 10^{10}$ VGs) with canal injections in adult mice¹⁹ found that most showed $<25\%$

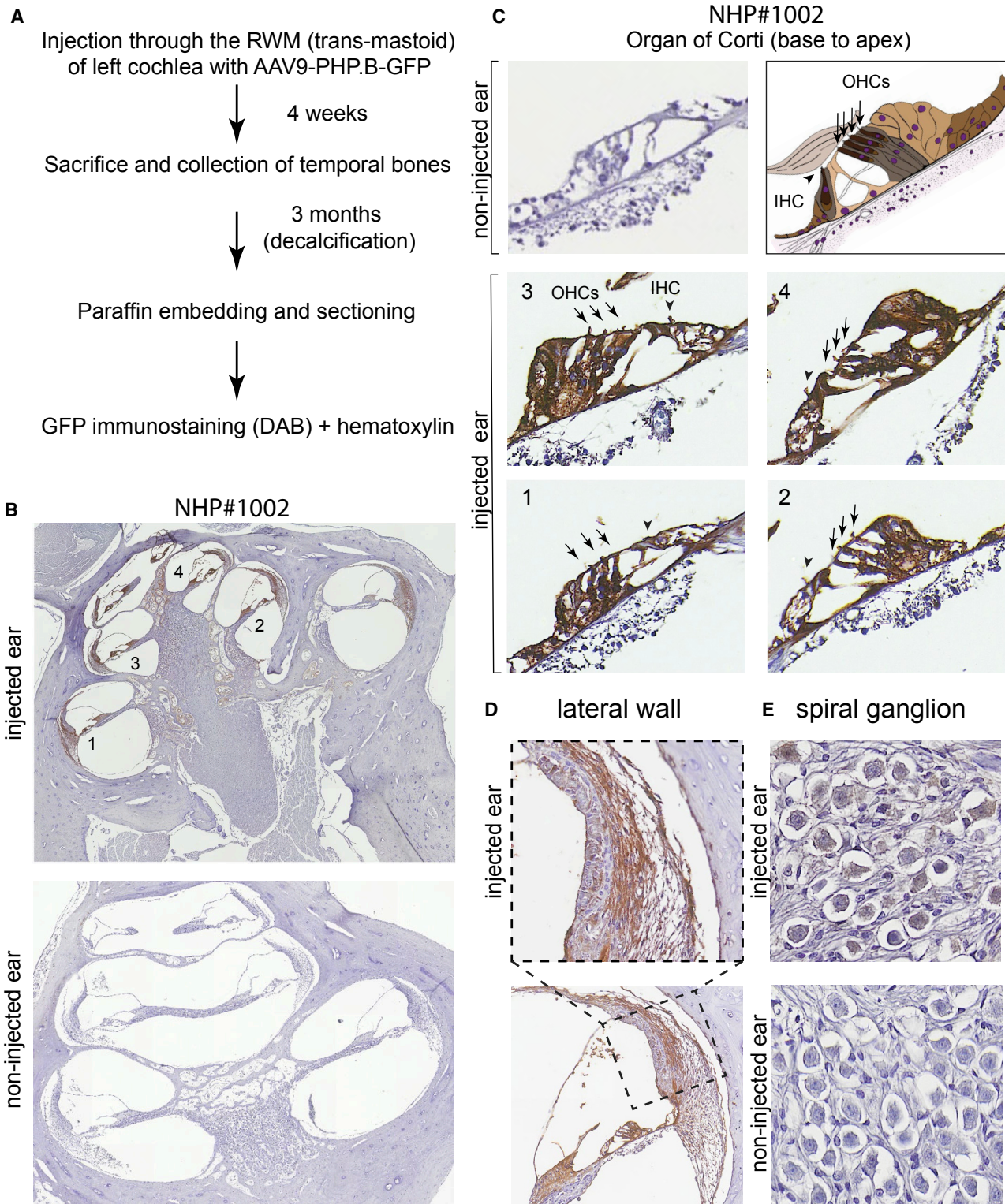


Figure 5. Transduction Profile of AAV9-PHP.B-CBA-GFP in the Cynomolgus Monkey (Animal #1002)

Vector (10 μ L; 3×10^{11} VGs) was injected through the RWM of a 2.6-year-old, 4-kg *Macaca fascicularis* monkey. (A) Experimental protocol. (B) Low-magnification images of the injected ear (top) and non-injected (bottom) ear. Anti-GFP staining was detected with a horseradish-peroxidase-conjugated secondary antibody and developed using

(legend continued on next page)

transduction of IHCs and little, if any, transduction in OHCs, with the exception of Anc80L65 (80%–100% IHCs and 2%–50% OHCs). In adult mice, canal injection of AAV9-PHP.B produced good transduction of IHCs but little efficacy in OHCs. Use of AAV9-PHP.B in mice for gene delivery to both IHCs and OHCs will likely be best for neonatal treatment.

Usher syndromes are characterized by the loss of both hearing and vision, so gene addition to retinal photoreceptors as well as HCs will be needed for comprehensive therapy. We observed that, with subretinal injection, AAV9-PHP.B transduces a large fraction of photoreceptors in adult mice (Figure 4). Gianelli et al.²⁰ found that the same vector transduces a substantial fraction of rods and cones with intravitreal injection as well.

Before clinical trials in humans, it will be necessary to show good efficacy in the cochlear HCs of a closely related primate. We found that AAV9-PHP.B transduced IHCs and OHCs in the cochlea of a juvenile male cynomolgus macaque (animal #1002) following RWM injection of 3×10^{11} VGs. Over 90% of both IHCs and OHCs were transduced in all sections from apex to base. In contrast, a second cynomolgus macaque (animal #3501, a juvenile female) showed extremely limited transduction, with no obvious transduction of HCs. One explanation of the discrepancy in transduction efficiency between the two animals could be dose related, as a 3-fold higher dose was utilized in animal #1002 that displayed efficient HC transduction. Other possible explanations are gender differences, genetic variability between animals, and the success of the RWM injections. Another unknown factor is whether pre-existing immunity to AAV (i.e., anti-AAV antibodies due to prior exposure to wild-type AAV) in perilymph can affect the transduction of cochlea. The two NHPs utilized in this study were not prescreened for anti-AAV antibodies, and future studies will need to be performed to evaluate whether transduction is inversely correlated with antibody titer, as has been observed with systemically and, sometimes, locally (intravitreal injection²¹) administered AAV. While these results demonstrate that it is feasible to transduce the inner ear of NHPs, further, extensive studies with larger group sizes are required to understand variables that may affect the transduction of various inner ear cell types.

The trans-mastoid surgical procedure in cynomolgus monkeys can be challenging, with the potential risk, as in humans, of damage to the facial nerve. The challenge of the surgery and visualization of proper insertion depth of the needle through the RWM is another possible explanation for the lower transduction in the second NHP (animal #3501). While the narrow ear canal of the macaque necessitates this alternate surgical approach, in humans, the RWM is easier to access using a trans-canal route. Despite the invasive trans-mastoid approach necessary for RWM injection in NHPs, the surgery was well

tolerated. Histological examination of animals post-injection revealed normal anatomical integrity, indicating minimal pathology related to the vector/surgery.

The high efficacy of AAV9-PHP.B in HCs of neonatal mice allowed partial rescue of hearing in a mouse knockout model of Usher 3A. Adult mice lacking a functional *Cln1* gene are profoundly deaf.^{13,22} With neonatal injection of AAV9-PHP.B encoding CLRN1, we achieved an increase of up to 50 dB in sensitivity, primarily in low-frequency regions. In Usher 3A mouse models that preserve expression of *Cln1* for a week or more after birth, better mimicking the human disease, other vectors encoding CLRN1 show efficient rescue of hearing,^{3,17} so we anticipate that AAV9-PHP.B will show even better rescue in these models. It is also important to note that Geng et al.³ tested a vector that included the 5' and 3' UTRs of murine *Clarin* and that this led to a greater rescue of hearing than the AAV-*Cln1* vector that did not contain the UTR. Thus, future work with AAV9-PHP.B-*Cln1* should contain the UTRs.

In conclusion, AAV9-PHP.B efficiently transduces the IHCs and OHCs of neonatal mouse and in one out of two injected NHPs. These data warrant further preclinical studies in NHPs to evaluate this vector as a potential candidate for cochlear gene therapy.

MATERIALS AND METHODS

AAV Vector Constructs

We used an AAV transgene plasmid, flanked by AAV2 inverted terminal repeats (ITRs), encoding GFP under the hybrid cytomegalovirus (CMV) immediate-early/CBA promoter, and with a woodchuck hepatitis virus posttranscriptional regulatory element (WPRE). This vector (AAV-CBA-GFP-W) encodes a ss genome. The helper plasmid pAdΔF6²³ was obtained from the Massachusetts General Hospital Vector Core. The pGG-PHP.B plasmid encoding the rep genes of AAV2 and the AAV9 variant, AAV9-PHP.B,⁹ was provided by Dr. Miguel Sena-Estevés (University of Massachusetts Medical School), who synthesized the capsid sequence based on the published sequence. We constructed an AAV ITR-containing plasmid encoding murine *Cln1*. The open reading frame of isoform 2 of *Cln2* was synthesized by GenScript (Piscataway, NJ, USA) and cloned into a ss AAV-expression (AAV-CBA-W) plasmid into the multiple cloning site to generate AAV-CBA-*Cln1*-W. We also had HA-tagged *Cln1* constructs synthesized (GenScript) and cloned them similarly into AAV-CBA-W.

To test whether the constructed plasmids expressed CLRN1, HEK293T cells were transiently transfected (calcium phosphate method) with each of the following plasmids in separate wells: AAV-CBA-*Cln1* (no tag), AAV-CBA-HA-*Cln1*, and AAV-CBA-*Cln1*-HA. AAV-HA-Lhfp15 was a previously characterized plasmid

diaminobenzidine (brown areas). Slides were counterstained with hematoxylin. (C) Higher magnification images of the organ of Corti from base to apex. The non-injected ear lacks GFP-specific immunoreactivity. The numbers in the cochlear turns in (B) correspond to panels 1–4. IHCs are indicated with arrowheads; OHCs are indicated with arrows. (D) Transduction of the lateral wall at high (top) and low (bottom) magnification. (E) Transduction of spiral ganglion neurons. We observed dim but consistent staining in the injected ear (top) but not the non-injected ear (bottom).

that we used as a negative control for *Clrn1* mRNA detection and a positive control for HA staining. Forty-eight hours post-transfection, a subset of wells was harvested for RNA harvest, while another set was harvested for immunofluorescence staining of the HA tag.

Vector Production and Purification

For each production, we plated ten 15-cm tissue culture dishes with 1.5×10^7 293T cells per dish. The next day, cells were transfected using the calcium phosphate method, with the adenovirus helper plasmid (pAd Δ F6, 26 μ g), rep/cap plasmid (pGG-PHP.B for AAV9-PHP.B, 12 μ g), and ITR-flanked transgene cassette plasmid (10 μ g) to induce production of AAV. The day after transfection, medium was changed to DMEM containing 2% fetal bovine serum (FBS). AAV was purified from the cell lysate using iodixanol density-gradient ultracentrifugation. Buffer exchange to PBS was conducted using Zeba spin columns (7K MWCO; Thermo Fisher Scientific) and further concentration was performed using Amicon Ultra 100-kDa MWCO ultrafiltration centrifugal devices (Millipore). Vectors were stored at -80°C until use. We quantified AAV genomic copies in AAV preparations using TaqMan qPCR with bovine growth hormone (BGH) poly(A) sequence-specific primers and probe.²⁴ During the course of this study, several independent preparations of AAV9-PHP.B vector were made, with each having slightly different titers. As we used the maximum injectable volume in each model (1.2 μ L for neonatal mice and 10 μ L for macaques), this resulted in differences in the dose between some experiments. All doses used are indicated in the figure legends and/or Results section.

Mouse Housing and Breeding

All experiments were performed in compliance with ethical regulations approved by the Animal Care Committee of Harvard Medical School (HMS). Wild-type pregnant C57BL/6 females were ordered from Charles River Laboratories, and pups were used for AAV-CBA-GFP transduction experiments. *Clrn1* knockout (KO) animals, in which the first coding exon was deleted,²¹ were a generous gift from Dr. Kumar Alagramam (Case Western Reserve University). Genotyping was done as previously described.²² They were housed and bred at the HMS animal facility.

Mouse RWM Injection in Neonatal Mice

P0–P1 CD1 and C57BL/6 pups were anesthetized by hypothermia and then kept on an ice pack during the procedure. As previously described,⁵ a small incision was made underneath the external ear. The incision was enlarged, and soft tissues were pushed apart using an eyelid retractor to expose the bulla. Then the round window niche was localized visually. Covering connective tissue was removed to expose the round window. For GFP expression experiments, we injected 1.0–1.2 μ L of AAV9-PHP.B-CBA-GFP vector solution at rate of 60 nL/min. For rescue experiments, we injected 1.0–1.2 μ L of the AAV9-PHP.B-CBA-*Clrn1* vector into the ear, which encodes CLRN1 without the HA tag. For immunostaining to detect CLRN1 encoded by the AAV, we used the vector encoding an N-terminal HA-tagged CLRN1. We closed surgical incisions with 2–3 sutures us-

ing a 7-0 Vycril surgical suture. After injection, we waited 5 days before sacrifice to assess vector transduction.

Adult Mouse Injection

4-week-old mice were anesthetized with ketamine (100 mg/kg) and xylazine (20 mg/kg) through an intraperitoneal injection. Both eyes were protected by an application of eye gel (GenTeal lubricant eye gel). The fur behind the left ear was shaved with a sterile razor, and the surgical area was cleansed two times with antiseptic solution, isolated with sterile drapes, and swabbed along the proposed incision with 10% povidone-iodine. We used a surgical procedure similar to that described by Suzuki et al.¹⁸ A small (10- to 15-mm) postauricular skin incision was made. After exposing the facial nerve and the sternocleidomastoid muscle by blunt dissection, the tissue covering the temporal was separated and retracted using the magnetic retractor set. A small hole was made with a microprobe in the exposed bony wall of the posterior canal. We waited 2–3 min for leakage of perilymph to stop, and then inserted the tip of a MicroFil 35G needle into the hole. The aperture between the MicroFil needle and the hole was sealed with tissue fragments and cyanoacrylate glue (3 M Vetbond Tissue Adhesive) and visually assessed for lack of fluid leakage. 1 μ L viral suspension at 155 nL/min was injected using the Nanoliter 2000 Injector (World Precision Instruments). After the injection was completed, the plastic needle remained in the canal for 5 min and then was cut off proximally to the canal. The hole was filled in with tissue and sealed with glue. The wound was closed with 5-0 Vicryl-coated sutures and swabbed with 10% povidone-iodine. The mouse was placed on a heating pad until full recovery. Animals received an intraperitoneal injection of meloxicam (0.01 mL/g body weight) after surgery and once more within the first 24 hr. Injected mice were checked daily for 5 days following surgery.

Mouse Cochlear Immunostaining and Imaging

For FM1-43 loading, organ of Corti epithelium was acutely dissected from P5 mice in L-15 cell culture medium and cultured for an additional day in DMEM supplemented with 5% FBS and ampicillin (10 mg/L). Following tectorial membrane removal and medium aspiration, FM1-43 solution (2 μ M in L-15) was applied to the tissue for 30–60 s and then quickly aspirated. The explant was then rinsed once with L-15, and the excessive dye was quenched by a 0.2 mM solution of 4-sulphonate calixarene, sodium salt (SCAS, Biotium), in L-15. The organ of Corti was then observed on an upright Olympus FV1000 confocal microscope, equipped with a 60 \times 1.1-NA water-dipping objective lens.

For immunostaining, cochleas were fixed with 4% formaldehyde in PBS for 20 min. Fixed cochleas were washed 3 times with PBS to remove fixative and were blocked with 5% normal goat serum and permeabilized with 0.3% Triton X-100 in PBS for 1 hr at 22 $^\circ\text{C}$. Primary antibodies were diluted in 5% normal goat serum (NGS)/0.1% Triton X-100/PBS and incubated overnight at 4 $^\circ\text{C}$. To label HCs, we used rabbit polyclonal anti-myosin VIIa antibody (Proteus Biosciences; 1:500 dilution) with a goat anti-rabbit immunoglobulin G (IgG) secondary antibody conjugated to Alexa Fluor 647 in a 1:1,000 dilution

for 1 hr (Life Technologies). To stain the hair bundle actin, we used phalloidin conjugated to Alexa Fluor 544 (Life Technologies) (1:50). To detect the HA tag, we used a rabbit anti-HA antibody (C29F4; Cell Signaling Technology). GFP was detected via its intrinsic fluorescence (i.e., no immunostaining for GFP). Tissues were mounted on a Colorfrost glass slide (Thermo Fisher Scientific) using Prolong Gold Antifade mounting medium (Thermo Fisher Scientific). Imaging for GFP fluorescence was performed with a Zeiss LSM 710 confocal microscope using a PlanApoN 60×/1.42-NA oil-immersion objective. For imaging to detect HA staining, we used an Olympus FluoView 1000 confocal microscope with a 60×/1.42-NA oil-immersion objective.

Quantification of EGFP Expression in Neonatal Murine HCs and Transduction Efficiency Analysis

Whole-mount cochleas, immunostained as described earlier, were imaged on a Zeiss LSM 710 for quantification in five different regions (apex, mid-apex, middle, mid-base, and base), each ~250 μm long along the axis of the organ of Corti and ~800 μm apart. The laser intensity was chosen based on the specimen with the strongest EGFP signal to prevent fluorescence saturation, and the same settings were then used for each image of a set. The efficiency of IHC and OHC cell transduction was evaluated by two blinded investigators using the ImageJ program (NIH Image). HCs were identified with immunolabeling for MYO7A. Control samples without AAV were used to exclude autofluorescence. Segments with dissection-related damage were removed from the analysis.

Mouse ABR

The ABR assay was performed using a Tucker Davis Technologies System III workstation. Mice were anesthetized by intraperitoneal injection of a ketamine (100 mg/kg)/xylazine (10 mg/kg) cocktail. Anesthetized mice were then placed on a heating pad, and electrodes were placed subcutaneously in the vertex, underneath the left or right ear, and on the back near the tail. Tone stimuli of 4, 5.6, 8, 11.2, 16, 22, 32, and 45.3 kHz were calibrated with a precision microphone system (PS9200 Kit; ACO Pacific), using the TDT SigCal software package. The recorded signals were band-pass filtered (300 Hz to 3 kHz) and amplified 100,000 times. The number of acquisition trials was set to 500 averages. Maximum stimulus intensity was set to 95 dB peak SPL with attenuation decreasing from 85 dB to 0 dB SPL at 5-dB intervals. Band-pass filters (500–3,000 Hz) were applied to the traces before analysis.

Mouse Retina

Animals were handled in accordance with the statement of the “Animals in Research Committee” of the Association for Research in Vision and Ophthalmology (Rockville, MD, USA), and protocols were approved by the local institutional committee (Service vétérinaire du canton de Vaud, Lausanne, Switzerland). Adult C57BL/6 mice were anesthetized with a reversible anesthetic regimen composed of ketamine and medetomidine (ketamine, 30–60 mg/kg, Parker Davis; medetomidine, 0.5–1 mg/kg, Graeb), and the anesthesia was reversed with the injection of atipamezole (0.5–1 mg/kg,

Graeb). For subretinal injections, a transcleral approach was used, and the procedure was visualized in the posterior chamber with a microscope and a coverslip covering the cornea surrounded with Visco-tears (Novartis, Basel, Switzerland). AAV9-PHP.B-CBA-GFP vector (1 μL) was injected into the sub-retinal space of adult mice through a Hamilton syringe with a 34G needle (BGB Analytik).

Scanning Electron Microscopy

Organ of Corti explants were dissected at P1 and P5 in L-15 medium and fixed with 2.5% glutaraldehyde in 0.1 M cacodylate buffer (pH 7.2) supplemented with 2 mM CaCl₂ for 1–2 hr at room temperature. For older (P30) animals, after intracardial perfusion with 4% paraformaldehyde and 1% glutaraldehyde, temporal bones were decalcified overnight in 10% EDTA (pH 7.2–7.4) for 3–4 days at 4°C. After unpeeling cochlear bone and removing the stria vascularis and tectorial membrane, the cochlear coils were isolated; divided into apical, middle, and basal turns; and postfixed with 2.5% glutaraldehyde in 0.1 M cacodylate buffer (pH 7.2) supplemented with 2 mM CaCl₂ for 1–2 hr at room temperature. They were rinsed three times in 0.1 M cacodylate buffer (pH 7.2), washed in distilled water, dehydrated in an ascending series of ethanol concentrations, and critical-point dried from liquid CO₂. Samples were then mounted on aluminum stubs with carbon conductive tabs and sputter-coated with 5 nm platinum, and then imaged in a field-emission scanning electron microscope (Hitachi S-4700).

Rat Cochlea

Sprague-Dawley rats (Charles River Laboratories) were injected at P1 through the RWM with 1.2 μL vector (ss AAV9-PHP.B-CBA-GFP) at an injection speed of 60 nL/min. The animals were allowed to recover from the injections; after 3 days, they were euthanized, and their cochleas were dissected. To assess vector transduction, organ of Corti explants were isolated, mounted on glass-bottom dishes, and cultured as previously described.⁵ Transduction was assessed on the day of the dissections (P4) or after 4 days in culture (P4+4) by visualizing the GFP fluorescence using confocal imaging.

NHP Cochlea

NHP studies were performed at Charles River Laboratories (Montreal, ON, Canada) according to animal use guidelines and approved procedures. The first cynomolgus monkey (*Macaca fascicularis*) (animal #1002) was a male, age 2.6 years, weighing 4 kg. The second animal (animal #3501) was a female, age 3.1 years, weighing 3.2 kg.

The animals were anesthetized by intramuscular injection of a cocktail (ketamine, 10 mg/kg; xylazine, 0.6 mg/kg; and glycopyrrolate, 0.01 mg/kg) following overnight food deprivation, intubated, and maintained with oxygen and isoflurane during surgery. During the procedure, the following were administered to improve recovery: warmed lactated Ringer's solution intravenously (10 ml/kg/hr), cefazolin (20 mg/kg every 20–90 min), and topical antibiotics to the surgical site. The RWM was exposed using a trans-mastoid approach. Beginning with a low microscopic magnification, the temporal muscles were retracted exposing the supramastoid crest and the external

cartilaginous portion of the ear canal. En route to the middle ear and with increasing magnification, mastoid air cells were burred very closely to the cartilaginous portion of the ear canal, and the bony portion thinned until the fossa incudis was reached, exposing the incus. A 1- to 2-mm facial recess was then performed with awareness of the horizontal semicircular canal, the facial nerve, and the tympanic membrane. The chorda tympani was retracted and/or resected, since it was not possible to preserve it without damaging the critical surrounding structures while allowing necessary exposure of the round window niche. In this species, the RWM is ~0.6 mm in diameter. Under micromanipulator control, a 29G injection needle was lowered through the RWM. For the first animal, vector (10 μ L) was injected with a pump at 0.5 μ L/min for 20 min, delivering 3×10^{11} VGs of AAV9-PHP.B-GFP into the right ear. The control left ear was uninjected. The second animal was injected in both ears with 10 μ L AAV9-PHP.B-GFP (1×10^{11} VGs per cochlea). Carprofen (4 mg/kg), Rimadyl (4 mg/kg), buprenorphine (sustained release [SR]: 0.2 mg/kg), and dexamethasone (0.75 mg/kg) were administered at appropriate intervals during the surgical recovery period. Animals were group housed during the observation period and monitored for reaction to treatment and body weight change.

Seven (animal #1002) or 8 (animal #3501) weeks post-surgery, the animal was euthanized, and temporal bones were excised. Tissue was fixed in neutral buffered 10% formalin for 48 hr and transferred to an EDTA solution for decalcification. Tissue was transferred to fresh solution and periodically scanned (Faxitron X-ray) until fully decalcified (~12 weeks) and then was embedded in paraffin, sectioned (5- μ m sections at 200- μ m intervals to reach the mid-modiolar cochlea), and mounted on glass slides. Slides were stained with H&E for histopathology evaluation or left unstained for immunohistochemistry.

Sections of cochlea were deparaffinized, using xylene followed by 100% and 95% ethanol washes, and then were rehydrated in water. Sections were permeabilized with 0.5% Triton X-100 in PBS for 30 min. Sections were blocked for endogenous peroxidase using 3% hydrogen peroxide for 10 min, washed, and then blocked using $1 \times$ Tris-buffered saline-Tween 20 (TBST)/5% normal goat serum for 1 hr at room temperature. Next, sections were incubated overnight at 4°C in primary antibody (anti-GFP antibody: GFP (D5.1) XP Rabbit mAb [monoclonal antibody], #2956, Cell Signaling Technology) at a 1:200 dilution in SignalStain antibody diluent (Cell Signaling Technology), and then they were washed and incubated in SignalStain Boost IHC Detection Reagent (horseradish peroxidase, rabbit #8114, Cell Signaling Technology) for 30 min at room temperature. After three washes, SignalStain diaminobenzidine (DAB) substrate was added to slides for 1–10 min until proper staining intensity had developed (in comparison to a negative control section such as secondary antibody only or uninjected cochlea). Slides were immersed in water and then counterstained with hematoxylin. Sections were washed in water, dehydrated with ethanol and xylene, and mounted using SignalStain mounting medium. Slides were viewed and digitized on an Olympus VS120 Virtual Slide Microscope.

Statistics

To compare two non-related sample groups, we used a t test for two independent samples or a Mann-Whitney U test. For normality testing, we used the Shapiro-Wilk test. For statistical testing, we used GraphPad Prism software. p values < 0.05 were considered statistically significant.

SUPPLEMENTAL INFORMATION

Supplemental Information includes nineteen figures and can be found with this article online at <https://doi.org/10.1016/j.omtm.2018.11.003>.

AUTHOR CONTRIBUTIONS

B.G. conceived of the study, carried out experiments, analyzed data, and wrote the manuscript. E.J.M. carried out experiments and analyzed data. M.V.I. carried out experiments, analyzed data, and wrote the manuscript. K.T. carried out experiments. F.E. carried out experiments. K.S.H. carried out experiments and analyzed data. A.A.I. carried out experiments and analyzed data. A.V. carried out experiments. K.D.K. carried out experiments. P.I.T. carried out experiments. M.V. conceived of the study. V.K.B. carried out experiments. R.T.B. carried out experiments. M.O. carried out experiments. J.-F.L. carried out experiments. Y.A. conceived of the study, carried out experiments, analyzed data, and wrote the manuscript. M.A.K. conceived of the study and carried out experiments. C.A.M. conceived of the study, carried out experiments, analyzed data, and wrote the manuscript. D.P.C. conceived of the study, carried out experiments, analyzed data, and wrote the manuscript.

CONFLICTS OF INTEREST

B.G., C.A.M., and D.P.C. are inventors on a pending patent application on use of AAV9-PHP.B for gene therapy in the inner ear. C.A.M. holds equity in and is a founder and scientific advisor of Chameleon Biosciences, a gene therapy company.

ACKNOWLEDGMENTS

We thank Dr. Kumar Alagramam for providing *Clrn1* knockout mice and Dr. Miguel Sena-Estevés for providing the plasmid encoding the PHP.B capsid. We appreciate assistance from Chester Chia in ABR recording and help from Brikha Shrestha in ABR recording. We greatly appreciate the management of mouse lines by Yaqiao Li. We also appreciate assistance from the MGH Quantitative Real-Time PCR Core, the HMS Neurobiology Imaging Facility (supported by NIH P30 grants EY12196 and NS072030), and the HMS MicRoN Microscopy Core. This work was supported by a Lefler Center postdoctoral fellowship (to B.G.); NIH grants DC002281 and DC016932 (to D.P.C.) R01DC017166 (to A.A.I.), and R01 EY11379 (to R.T.B.); a Partners Innovation Discovery Fund grant (to C.A.M.); and a Cure Alzheimer's Disease Fund grant (to C.A.M.). B.G. was an associate, and D.P.C. was an investigator of the Howard Hughes Medical Institute. We appreciate institutional support to Harvard Medical School from the Bertarelli Foundation.

REFERENCES

- Akil, O., Seal, R.P., Burke, K., Wang, C., Alemi, A., During, M., Edwards, R.H., and Lustig, L.R. (2012). Restoration of hearing in the VGLUT3 knockout mouse using virally mediated gene therapy. *Neuron* 75, 283–293.
- Askew, C., Rochat, C., Pan, B., Asai, Y., Ahmed, H., Child, E., Schneider, B.L., Aebischer, P., and Holt, J.R. (2015). Tmc gene therapy restores auditory function in deaf mice. *Sci. Transl. Med.* 7, 295ra108.
- Geng, R., Omar, A., Gopal, S.R., Chen, D.H., Stepanyan, R., Basch, M.L., Dinculescu, A., Furness, D.N., Saperstein, D., Hauswirth, W., et al. (2017). Modeling and preventing progressive hearing loss in Usher syndrome III. *Sci. Rep.* 7, 13480.
- Chien, W.W., Isgrig, K., Roy, S., Belyantseva, I.A., Drummond, M.C., May, L.A., Fitzgerald, T.S., Friedman, T.B., and Cunningham, L.L. (2016). Gene therapy restores hair cell stereocilia morphology in inner ears of deaf whirler mice. *Mol. Ther.* 24, 17–25.
- György, B., Sage, C., Indzhykalian, A.A., Scheffer, D.I., Brisson, A.R., Tan, S., Wu, X., Volak, A., Mu, D., Tamvakologos, P.I., et al. (2017). Rescue of hearing by gene delivery to inner-ear hair cells using exosome-associated AAV. *Mol. Ther.* 25, 379–391.
- Landegger, L.D., Pan, B., Askew, C., Wassmer, S.J., Gluck, S.D., Galvin, A., Taylor, R., Forge, A., Stankovic, K.M., Holt, J.R., and Vandenberghe, L.H. (2017). A synthetic AAV vector enables safe and efficient gene transfer to the mammalian inner ear. *Nat. Biotechnol.* 35, 280–284.
- Pan, B., Askew, C., Galvin, A., Heman-Ackah, S., Asai, Y., Indzhykalian, A.A., Jodelka, F.M., Hastings, M.L., Lentz, J.J., Vandenberghe, L.H., et al. (2017). Gene therapy restores auditory and vestibular function in a mouse model of Usher syndrome type 1c. *Nat. Biotechnol.* 35, 264–272.
- Zhang, W., Kim, S.M., Wang, W., Cai, C., Feng, Y., Kong, W., and Lin, X. (2018). Cochlear gene therapy for sensorineural hearing loss: current status and major remaining hurdles for translational success. *Front. Mol. Neurosci.* 11, 221.
- Deverman, B.E., Pravdo, P.L., Simpson, B.P., Kumar, S.R., Chan, K.Y., Banerjee, A., Wu, W.L., Yang, B., Huber, N., Pasca, S.P., and Gradinaru, V. (2016). Cre-dependent selection yields AAV variants for widespread gene transfer to the adult brain. *Nat. Biotechnol.* 34, 204–209.
- Hordeaux, J., Wang, Q., Katz, N., Buza, E.L., Bell, P., and Wilson, J.M. (2018). The neurotropic properties of AAV-PHP.B are limited to C57BL/6J mice. *Mol. Ther.* 26, 664–668.
- Scheffer, D.I., Shen, J., Corey, D.P., and Chen, Z.Y. (2015). Gene expression by mouse inner ear hair cells during development. *J. Neurosci.* 35, 6366–6380.
- Geller, S.F., Guerin, K.I., Visel, M., Pham, A., Lee, E.S., Dror, A.A., Avraham, K.B., Hayashi, T., Ray, C.A., Reh, T.A., et al. (2009). CLRN1 is nonessential in the mouse retina but is required for cochlear hair cell development. *PLoS Genet.* 5, e1000607.
- Geng, R., Melki, S., Chen, D.H., Tian, G., Furness, D.N., Oshima-Takago, T., Neef, J., Moser, T., Askew, C., Horwitz, G., et al. (2012). The mechanosensory structure of the hair cell requires clarin-1, a protein encoded by Usher syndrome III causative gene. *J. Neurosci.* 32, 9485–9498.
- Dai, C., Lehar, M., Sun, D.Q., Rvt, L.S., Carey, J.P., MacLachlan, T., Brough, D., Staecker, H., Della Santina, A.M., Hullar, T.E., and Della Santina, C.C. (2017). Rhesus cochlear and vestibular functions are preserved after inner ear injection of saline volume sufficient for gene therapy delivery. *J. Assoc. Res. Otolaryngol.* 18, 601–617.
- Lisowski, L., Dane, A.P., Chu, K., Zhang, Y., Cunningham, S.C., Wilson, E.M., Nygaard, S., Grompe, M., Alexander, I.E., and Kay, M.A. (2014). Selection and evaluation of clinically relevant AAV variants in a xenograft liver model. *Nature* 506, 382–386.
- Matsuzaki, Y., Konno, A., Mochizuki, R., Shinohara, Y., Nitta, K., Okada, Y., and Hirai, H. (2018). Intravenous administration of the adeno-associated virus-PHP.B capsid fails to upregulate transduction efficiency in the marmoset brain. *Neurosci. Lett.* 665, 182–188.
- Dulon, D., Papal, S., Patni, P., Cortese, M., Vincent, P.F., Tertrais, M., Emptoz, A., Tlili, A., Bouleau, Y., Michel, V., et al. (2018). Clarin-1 gene transfer rescues auditory synaptopathy in model of Usher syndrome. *J. Clin. Invest.* 128, 3382–3401.
- Suzuki, J., Hashimoto, K., Xiao, R., Vandenberghe, L.H., and Liberman, M.C. (2017). Cochlear gene therapy with ancestral AAV in adult mice: complete transduction of inner hair cells without cochlear dysfunction. *Sci. Rep.* 7, 45524.
- Tao, Y., Huang, M., Shu, Y., Ruprecht, A., Wang, H., Tang, Y., Vandenberghe, L.H., Wang, Q., Gao, G., Kong, W.J., and Chen, Z.Y. (2018). Delivery of adeno-associated virus vectors in adult mammalian inner-ear cell subtypes without auditory dysfunction. *Hum. Gene Ther.* 29, 492–506.
- Giannelli, S.G., Luoni, M., Castoldi, V., Massimino, L., Cabassi, T., Angeloni, D., Demontis, G.C., Leocani, L., Andreatzoli, M., and Broccoli, V. (2018). Cas9/sgRNA selective targeting of the P23H Rhodopsin mutant allele for treating retinitis pigmentosa by intravitreal AAV9.PHP.B-based delivery. *Hum. Mol. Genet.* 27, 761–779.
- Kotterman, M.A., Yin, L., Strazzeri, J.M., Flannery, J.G., Merigan, W.H., and Schaffer, D.V. (2015). Antibody neutralization poses a barrier to intravitreal adeno-associated viral vector gene delivery to non-human primates. *Gene Ther.* 22, 116–126.
- Geng, R., Geller, S.F., Hayashi, T., Ray, C.A., Reh, T.A., Bermingham-McDonogh, O., Jones, S.M., Wright, C.G., Melki, S., Imanishi, Y., et al. (2009). Usher syndrome IIIA gene clarin-1 is essential for hair cell function and associated neural activation. *Hum. Mol. Genet.* 18, 2748–2760.
- Xiao, X., Li, J., and Samulski, R.J. (1998). Production of high-titer recombinant adeno-associated virus vectors in the absence of helper adenovirus. *J. Virol.* 72, 2224–2232.
- Maguire, C.A., Balaj, L., Sivaraman, S., Crommentuijn, M.H., Ericsson, M., Mincheva-Nilsson, L., Baranov, V., Gianni, D., Tannous, B.A., Sena-Esteves, M., et al. (2012). Microvesicle-associated AAV vector as a novel gene delivery system. *Mol. Ther.* 20, 960–971.

Supplemental Information

Gene Transfer with AAV9-PHP.B Rescues Hearing in a Mouse Model of Usher Syndrome 3A and Transduces Hair Cells in a Non-human Primate

Bence György, Elise J. Meijer, Maryna V. Ivanchenko, Kelly Tenneson, Frederick Emond, Killian S. Hanlon, Artur A. Indzhukulian, Adrienn Volak, K. Domenica Karavitaki, Panos I. Tamvakologos, Mark Vezina, Vladimir K. Berezovskii, Richard T. Born, Maureen O'Brien, Jean-François Lafond, Yvan Arsenijevic, Margaret A. Kenna, Casey A. Maguire, and David P. Corey

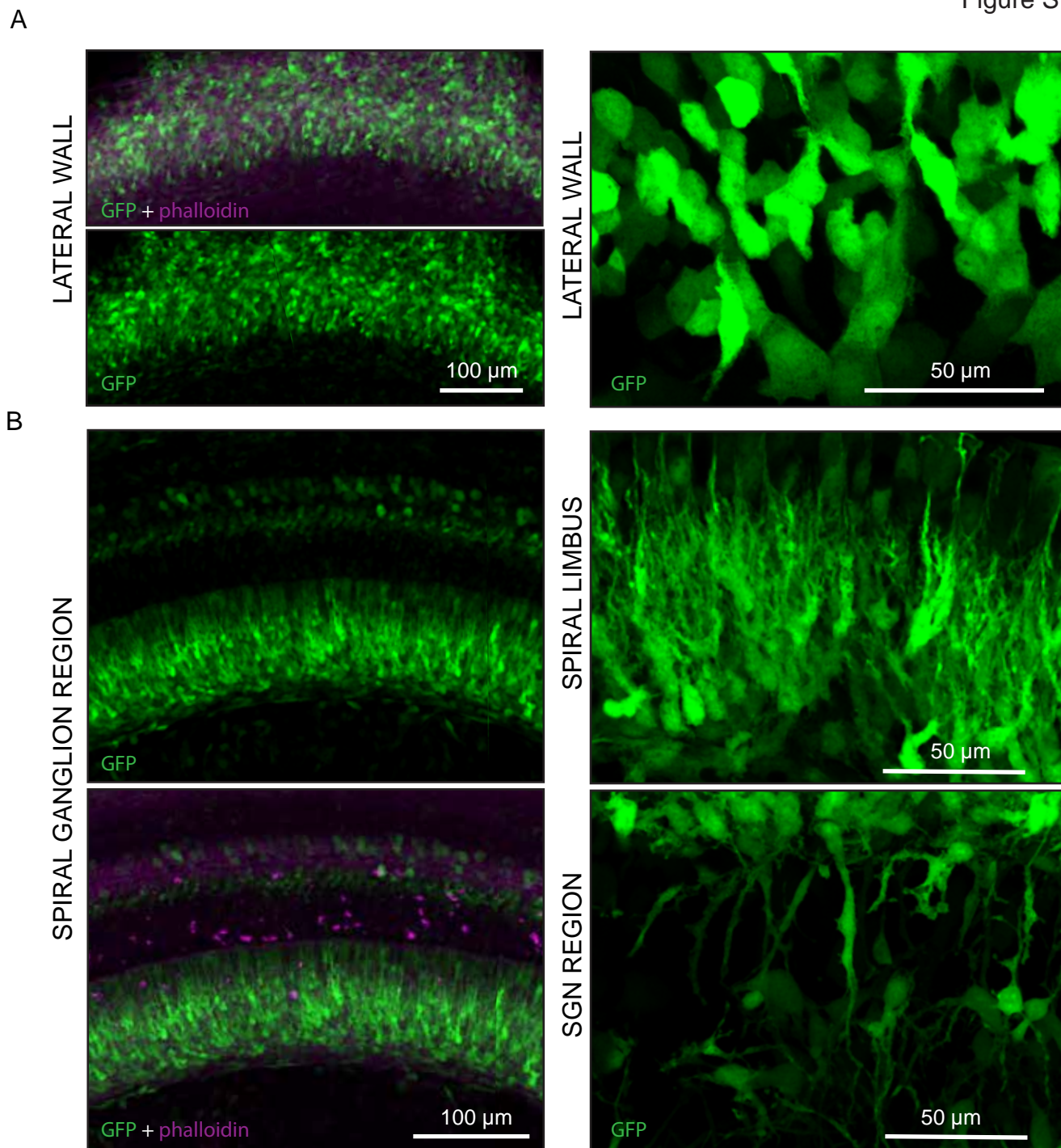


Figure S1. Transduction efficiency of AAV9-PHP.B-CBA-GFP in the lateral wall and spiral ganglion region of the cochlea, after neonatal RWM injection. (A) C57BL/6J mice were injected at P1 with 5×10^{10} vector genomes, cochleas were explanted at P5, and cultured for one more day (P5+1). Low magnification (left panel) and high magnification (right panel) images of the lateral wall. Left panel shows GFP together with phalloidin staining of actin (top) and GFP staining only (bottom); right panel shows GFP. (B) Low magnification images of spiral ganglion region (left) and high magnification images of spiral limbus and spiral ganglion neurons (SGN) region.

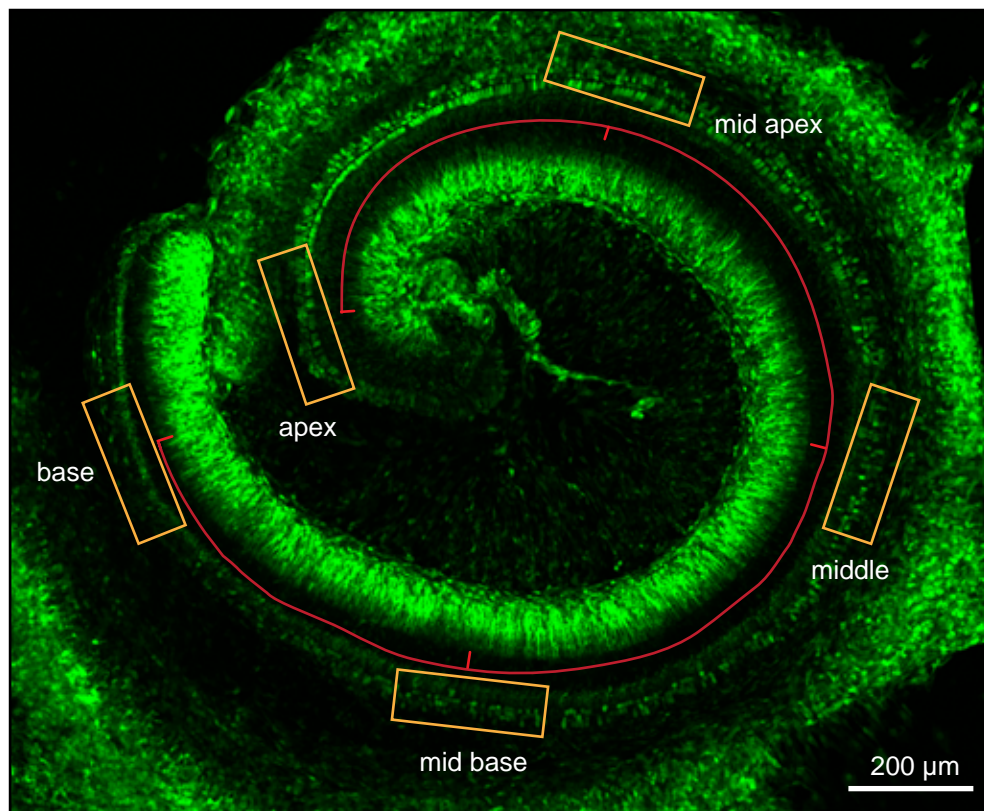


Figure S2. Quantification method for determination of transduction efficiency in specified cochlear regions. Transduction efficiencies in IHCs and OHCs were quantified in 5 different regions (apex, mid apex, middle, mid base, base (yellow boxes). The regions were ~800 μm apart from each other (red trace).

Right cochlea (non injected ear) WT (C57BL/6J)

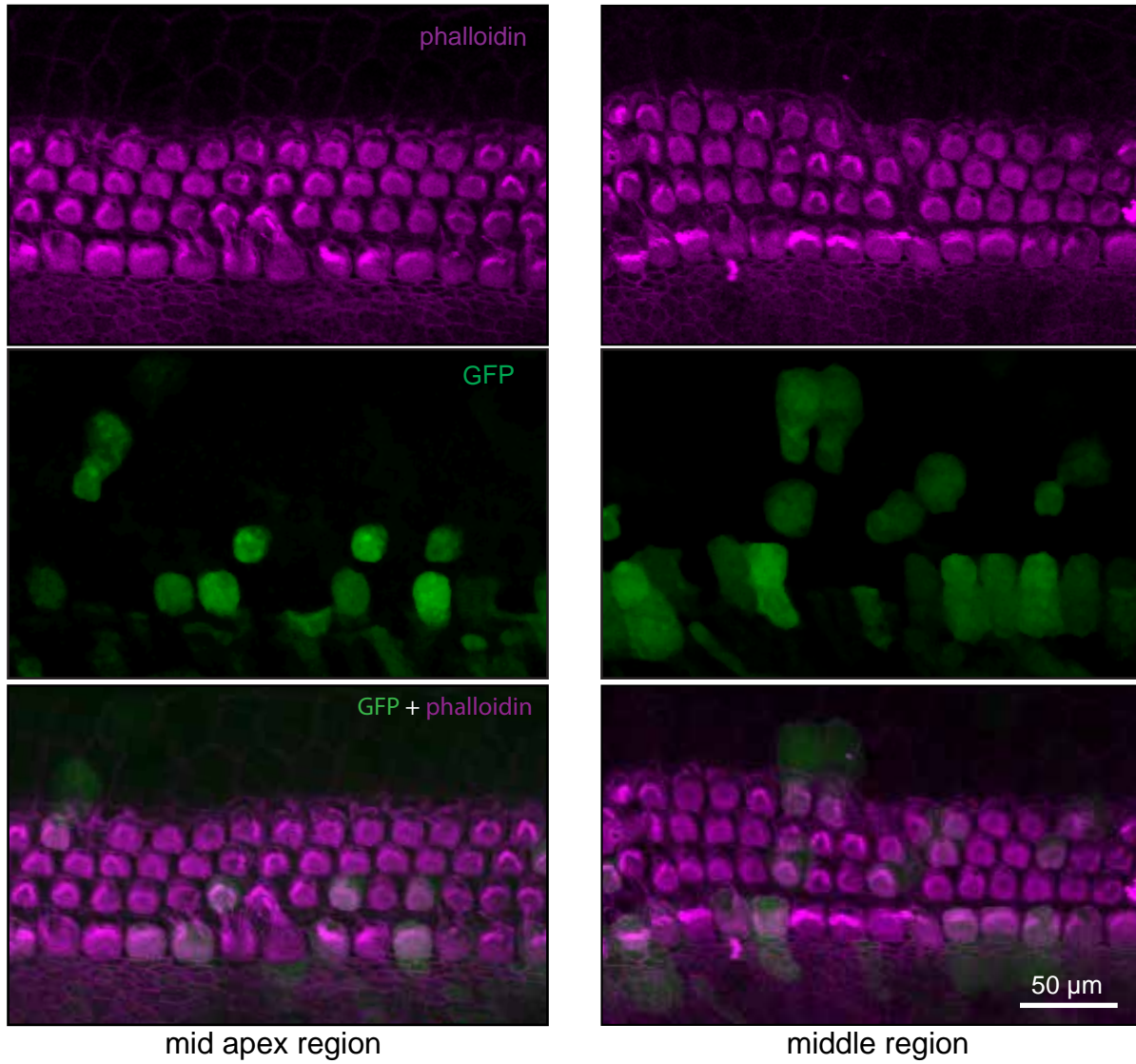


Figure S3. Transduction of AAV9-PHP.B-CBA-GFP in a non-injected ear of a C57BL/6J mouse after neonatal round window membrane (RWM) injection to the contralateral ear. Left panels (mid apex region) and right panels (middle region) show GFP expression in some IHCs and OHC.

Adult injection (C57BL/6J)

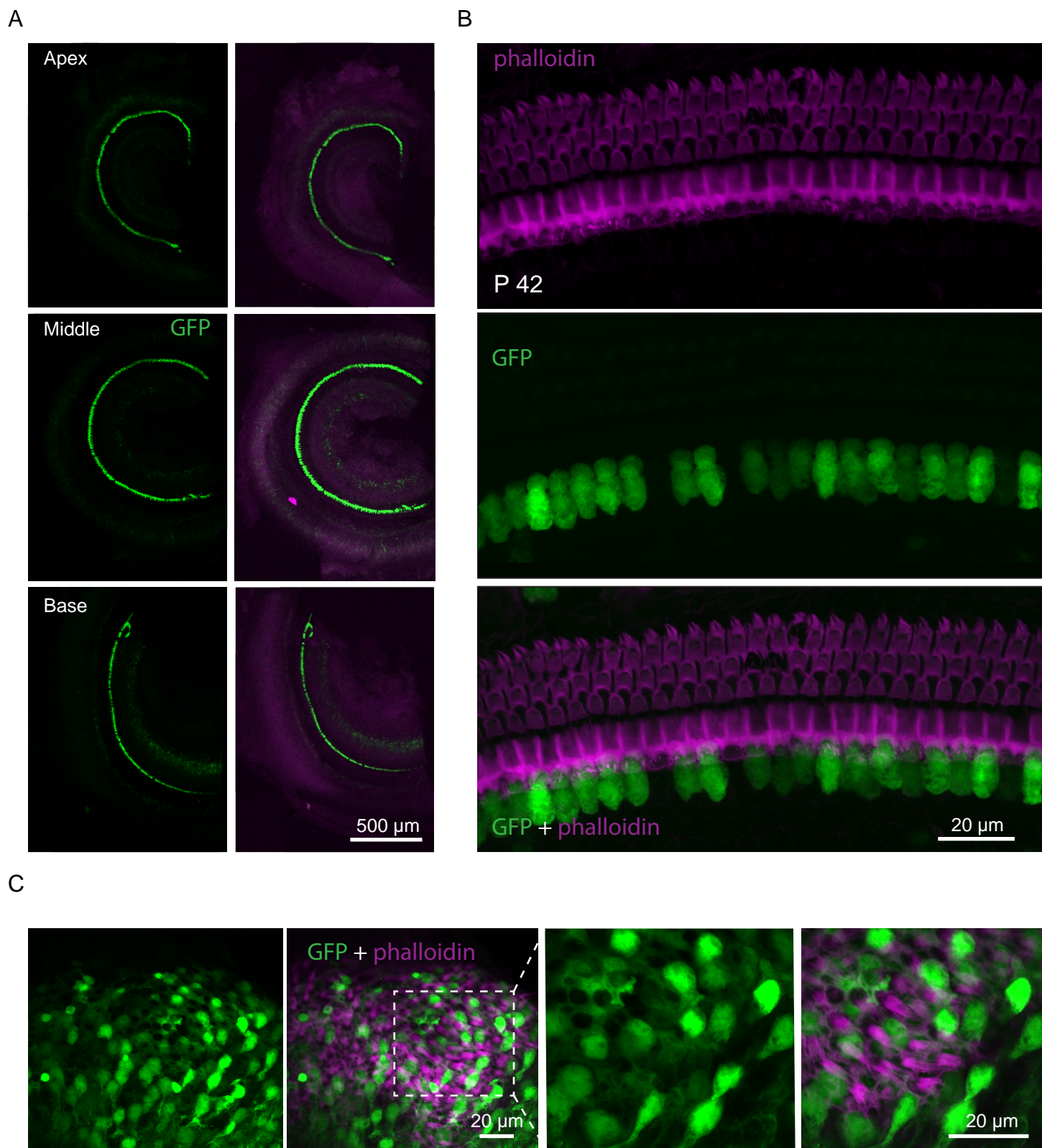
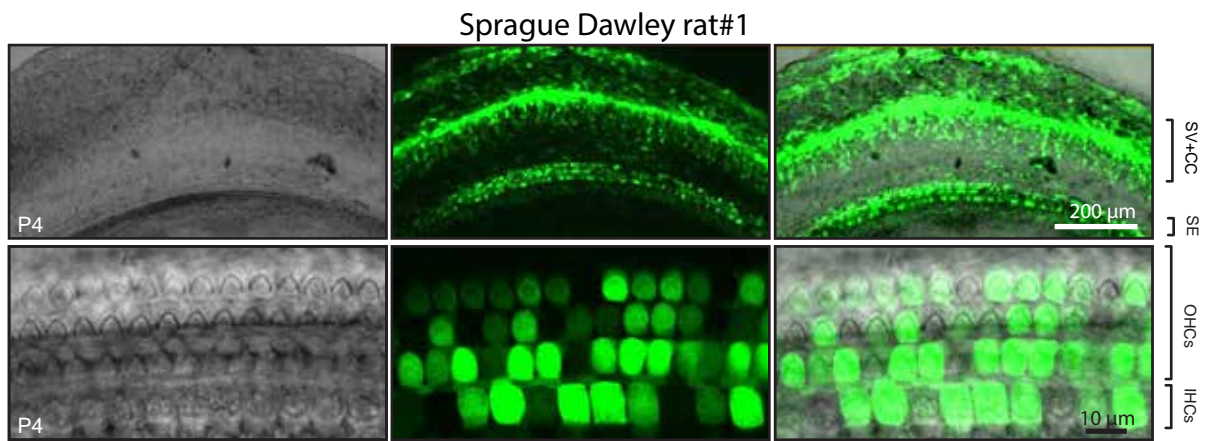


Figure S4. Transduction of adult hair cells by AAV9-PHP.B-CBA-GFP in C57BL/6J mice after injection at P28 through the posterior semicircular canal. Four-week old animals were injected with 2×10^{10} vector genomes. At P42 (2 weeks after injection), transduction was observed in almost all IHCs, but not in OHCs. **(A)** Low magnification images of the apical, middle and basal turns of the cochlea. **(B)** High magnification images of middle region of the cochlea with the high transduction in the IHCs. **(C)** AAV9-PHP.B-CBA-GFP transduces cells in the vestibular system (utricle).

A



B

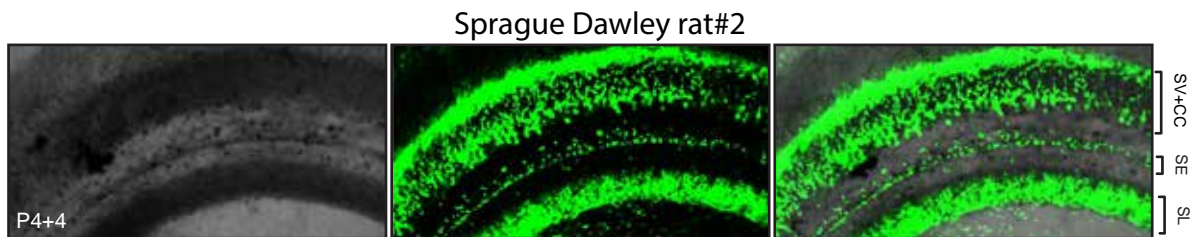


Figure 5. Transduction efficiency in Sprague Dawley rats of AAV9-PHP.B-CBA-GFP after neonatal RWM injection. Transduction efficiency of AAV9-PHP.B-CBA-GFP after neonatal round window membrane injection in rat#1 and rat#2 (**A, B**). Live cell imaging was performed in explanted cochleas at P4 for the rat#1 (**A**) and P4+4 days in culture for the rat #2 (**B**). Lower magnification images are shown on the top (**A, B**) and higher magnification at the bottom (**A**). Left panels show DIC imaging to visualize hair bundles.

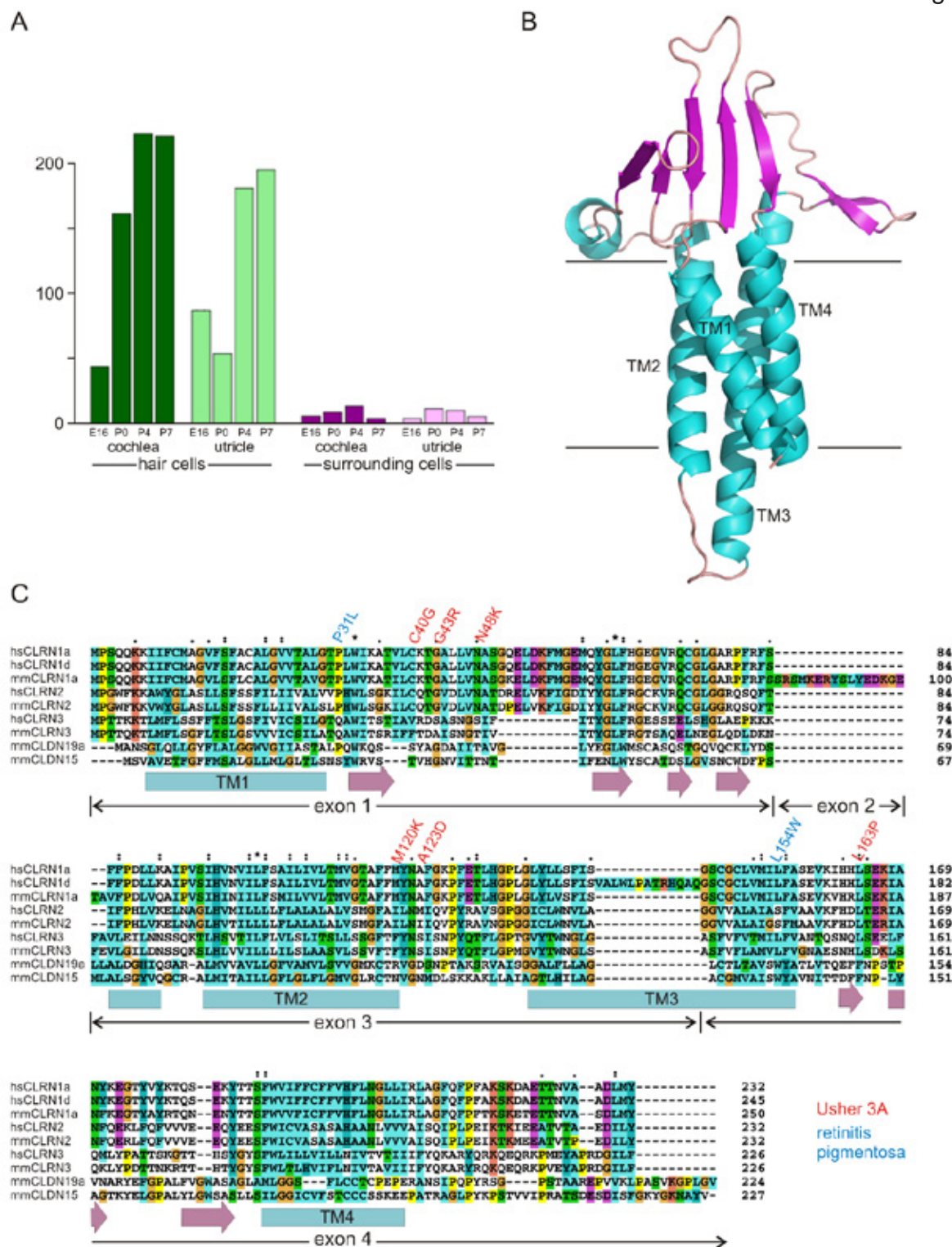


Figure S6. Expression, predicted structure and sequence alignment for CLRN1-related proteins. (A) Expression of *Clrn1* in mouse inner ear, from Scheffer et al. (2015). mRNA levels rise around the time that hair cells gain mechanosensitivity, but there is little expression in surrounding cells. (B) Predicted structure of hsCLRN1 based on known structures of CLDN19 and CLDN15 (Phyre2; Kelly et al., 2015). (C) Alignment of human and mouse CLRN1 splice forms with mouse CLDN19 and CLDN15. Mutations in hsCLRN1 producing Usher syndrome 3A or retinitis pigmentosa alone are indicated.

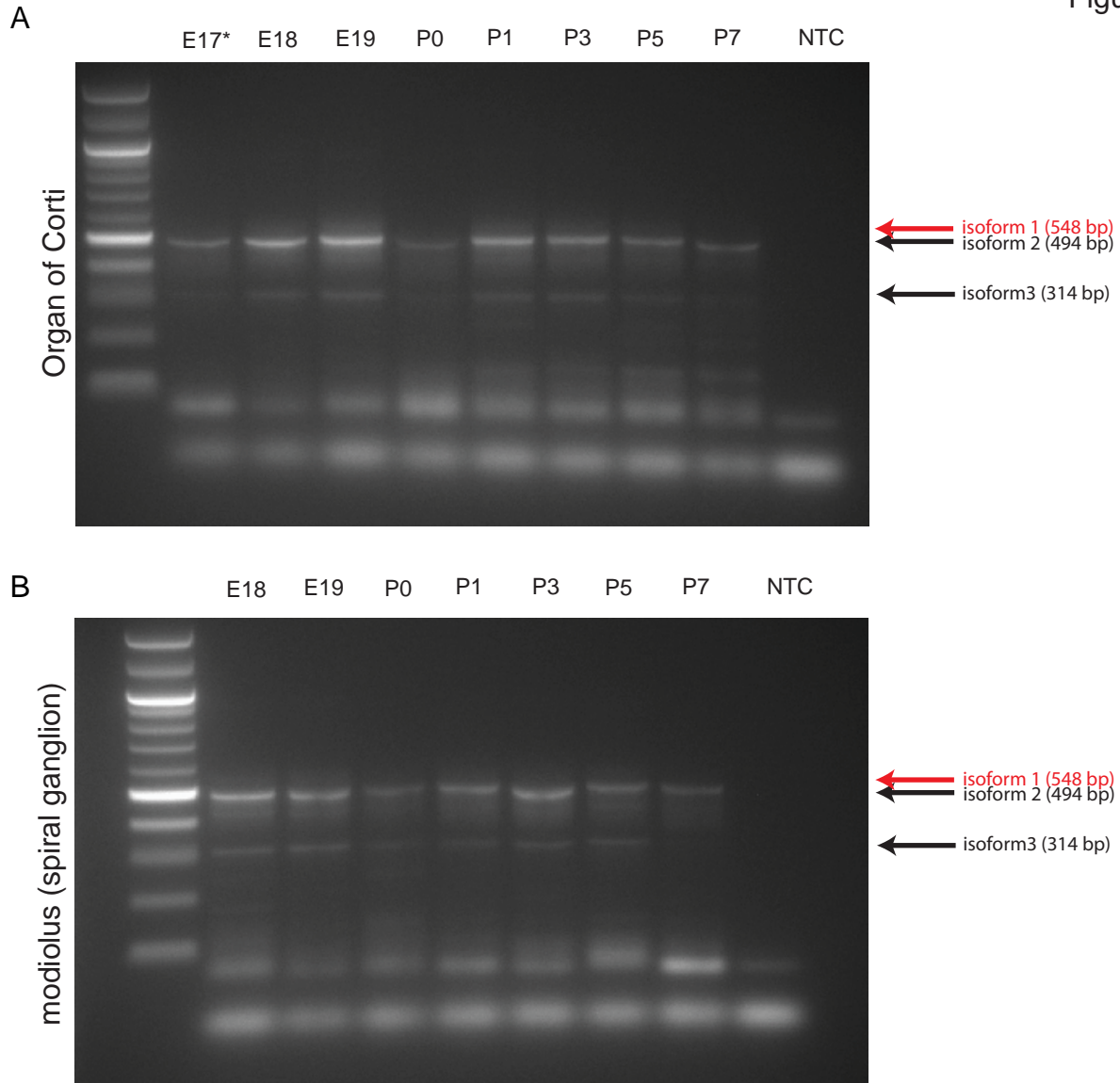


Figure S7. Clarin-1 expression and isoform analysis from E17 to P7. RNA was isolated from from the organ of (A) Corti region and (B) spiral ganglion region at different stages of development. Whole cochlea was used at E17. RT-PCR was performed using primers in exon 1 and exon 4. PCR products were run on a 1% agarose gel. Isoforms and sizes are shown on the right. For size comparison, we used a 100bp ladder from NEB.

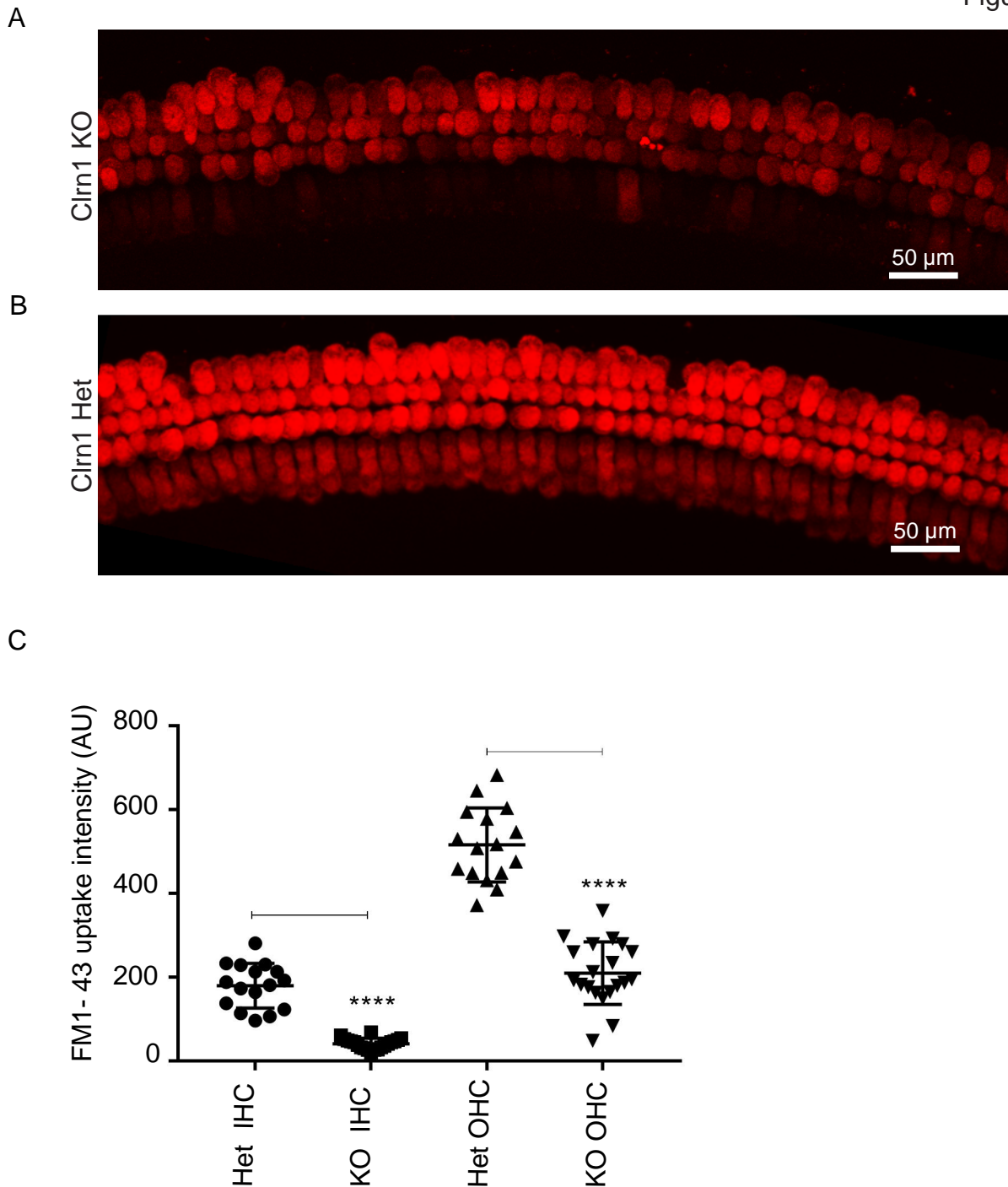


Figure S8. FM1-43 loading in hair cells from *Clrn1* heterozygous (Het) and homozygous (KO) knockout mice. (A, B) Confocal microscopy images of FM1-43-loaded hair cells in KO and Het mice. (C) FM1-43 signal intensity measured with ImageJ. In *Clrn1* KO mice, FM1-43 intensity was significantly lower than in heterozygotes, in both IHCs and OHCs. Unpaired t-test for all regions combined; $p < 0.0001$ for both IHCs and OHCs.

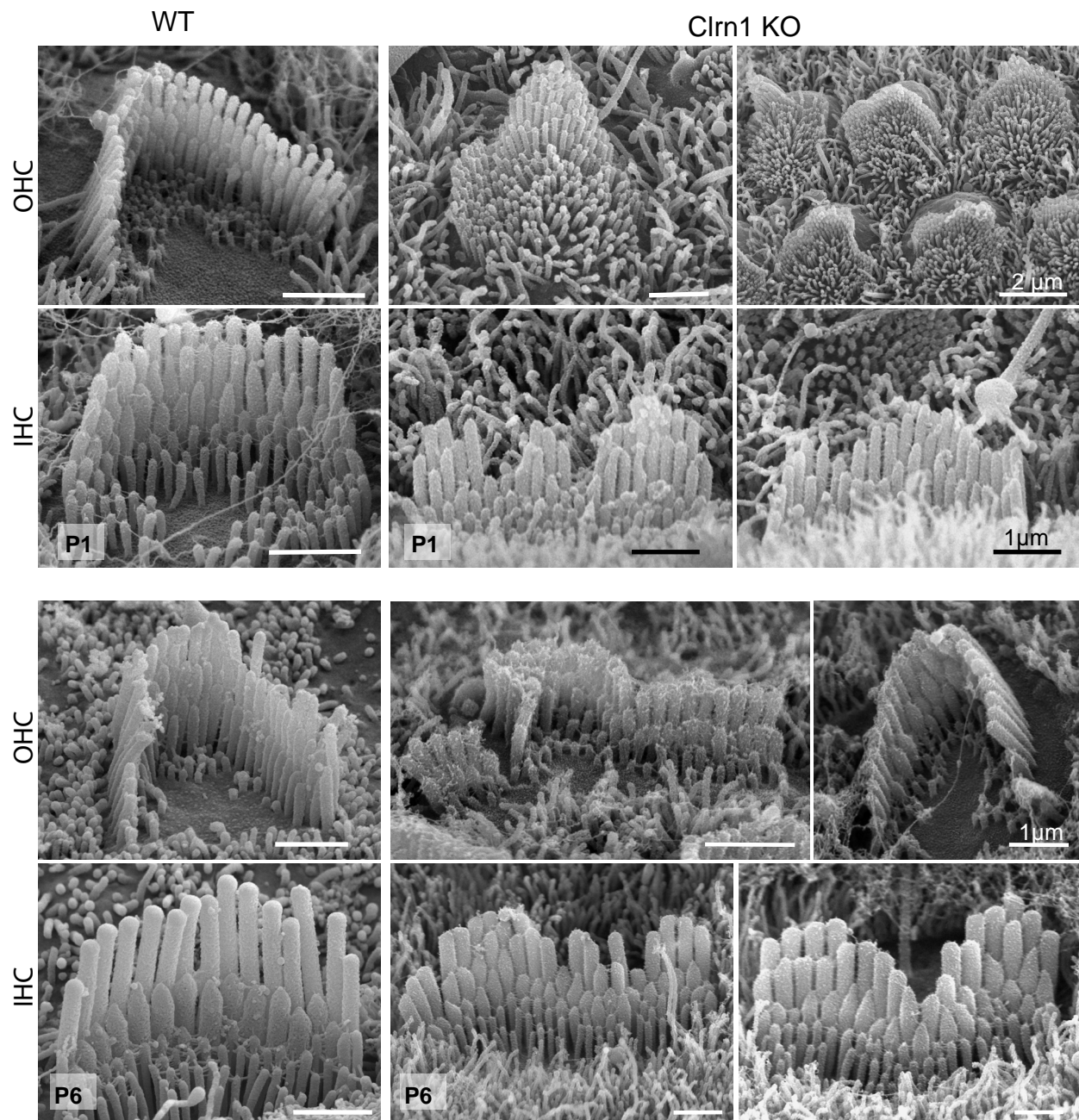


Figure S9. SEM images of organ of Corti from mid-cochlear regions, from WT and *Cln1* KO mice. SEM analysis of *Cln1* KO revealed loss of orientation and disorganization of hair bundles compared to the WT hair cells at, beginning as early as P1 and progressing at P6, with separation of columns, missing and shortened stereocilia, and distorted tips.

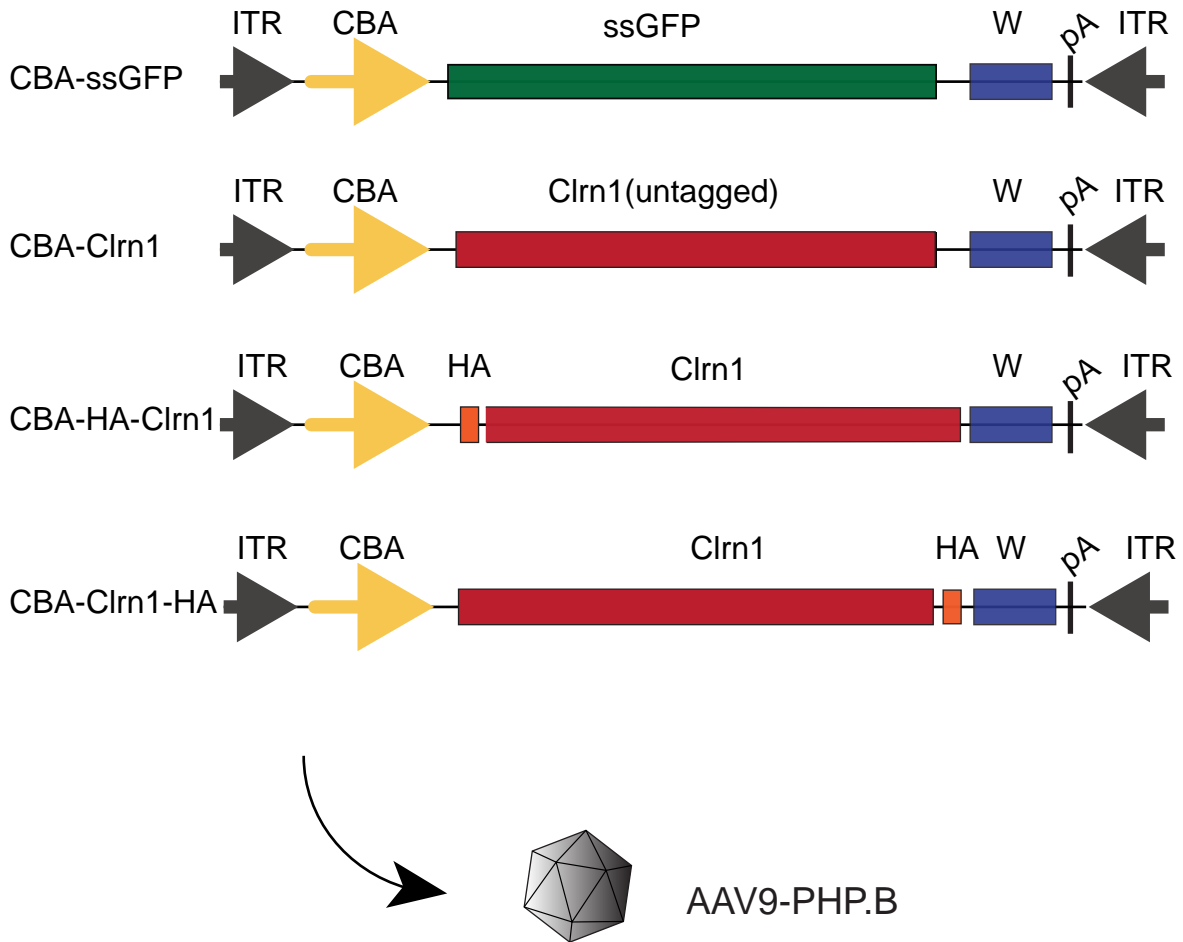


Figure S10. Schematics of the AAV vectors used in the study. From top: GFP vector, untagged clarin-1 vector, N-terminal HA-tagged clarin-1 vector, and C-terminal HA-tagged clarin-1 vector. All vectors are single stranded. ITR: inverted terminal repeat, CBA: chicken beta-actin promoter, HA: hemagglutinin tag, W: WPRE element (woodchuck hepatitis virus posttranscriptional regulatory element), pA: BGH poly A signal.

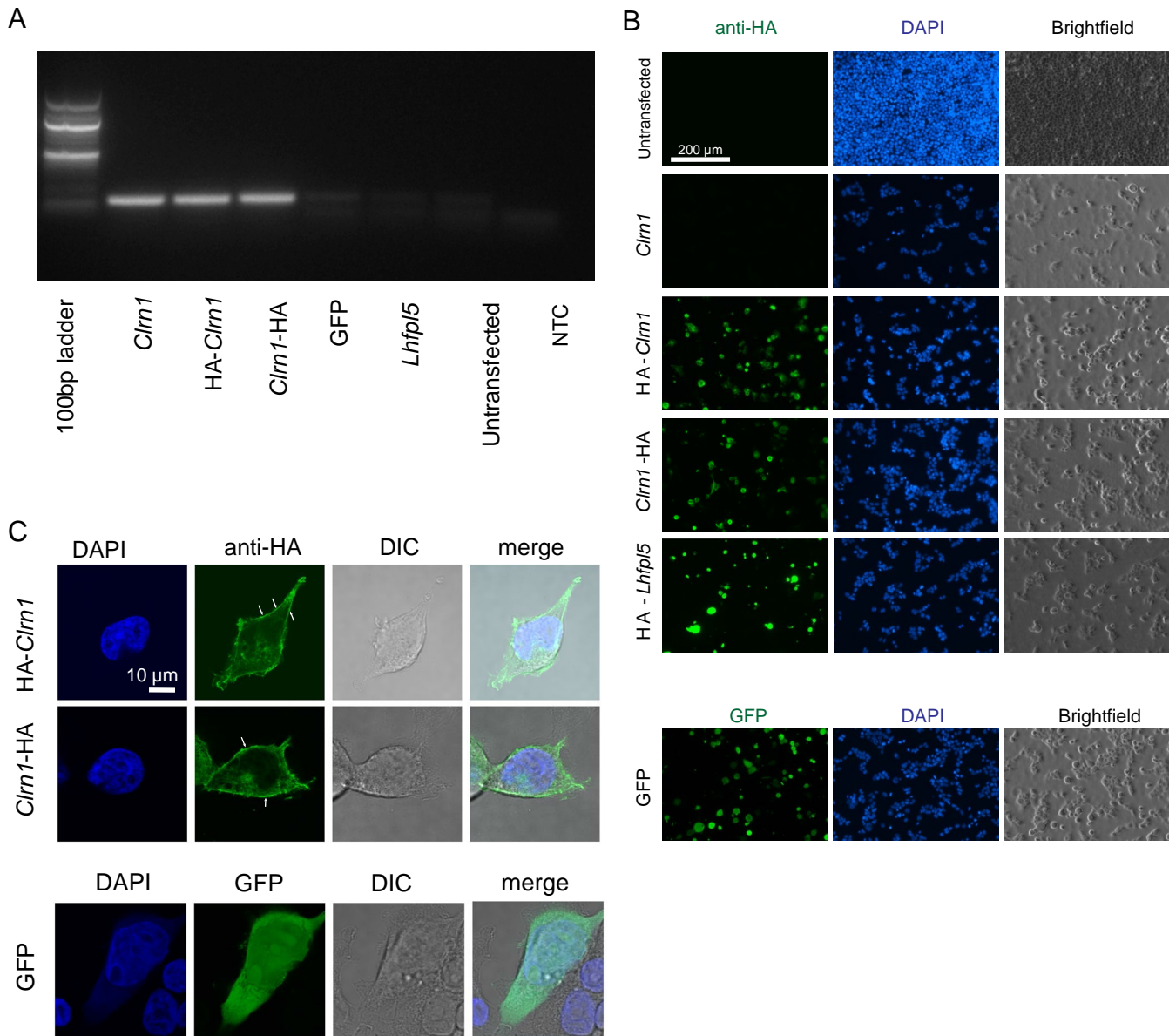
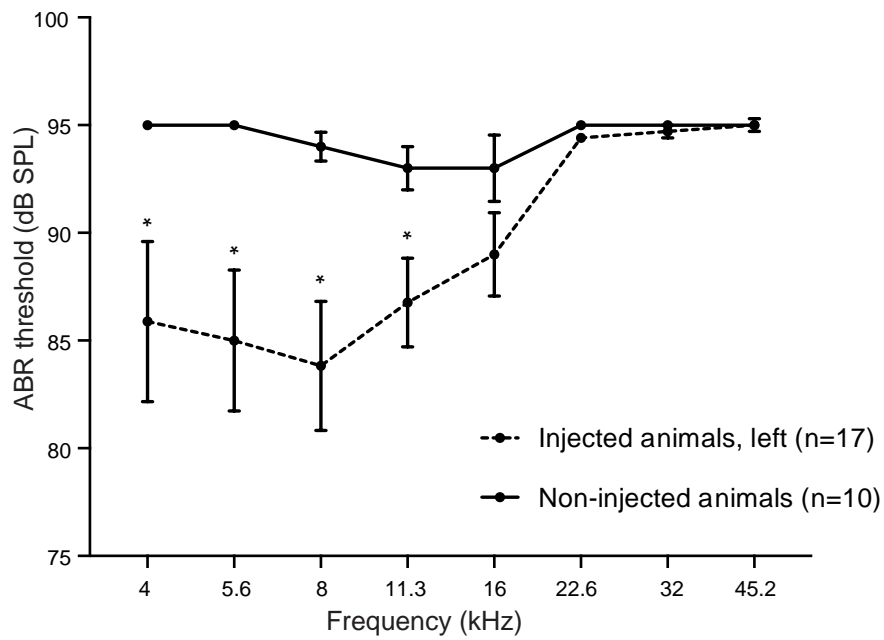


Figure S11. Clarin-1 expression in HEK cells. Cells were transfected with CBA-*Clrn1*, CBA-HA-*Clrn1*, CBA-*Clrn1*-HA, CBA-GFP and CBA-HA-*Lhfp15* AAV plasmids. (A) RT-PCR products were run on an 1% agarose gel; expected product size is 171 bp. (B) Immunostaining for HA or native GFP fluorescence. (C) High magnification confocal images; HA staining or GFP fluorescence.

A Cln1 KO, 4 weeks, AAV.PHP.B-CBA-Cln1 injected vs non-injected



B

Cln1 KO, 4 weeks, AAV.PHP.B-CBA-Cln1 injected, left vs right

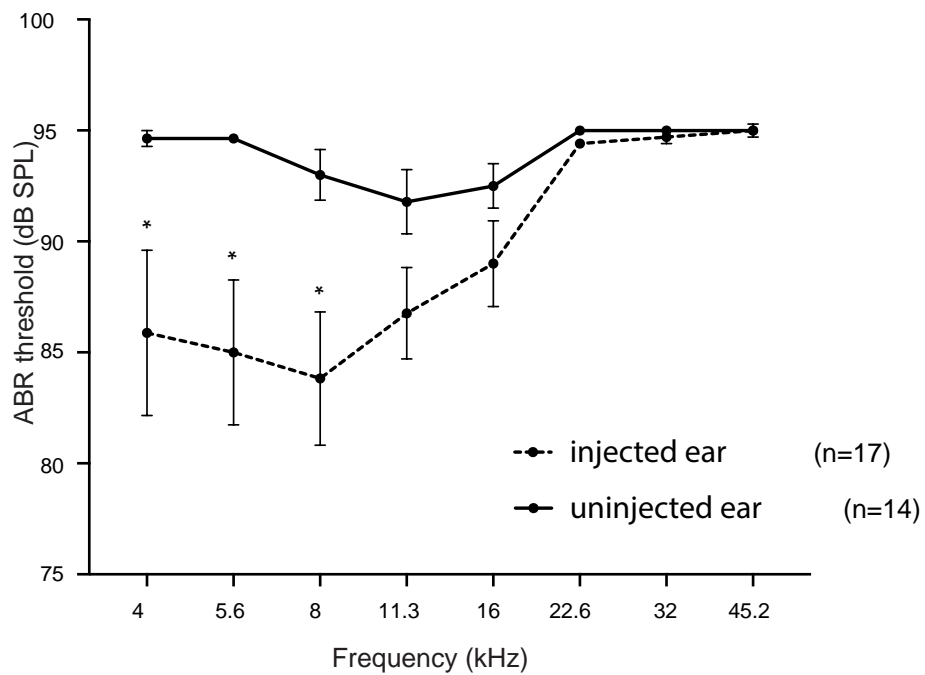
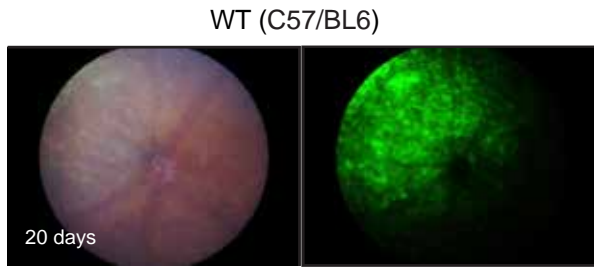


Figure S12. AAV9-PHP.B-Clarín mediated rescue of hearing in Cln1 KO animals is significantly better than (A) non-injected mice and (B) injected ear (left) vs. uninjected (right) ear. Both (A) and (B) are from the same data described in Figure 3. $p < 0.05$, Wilcoxon test.

A



B

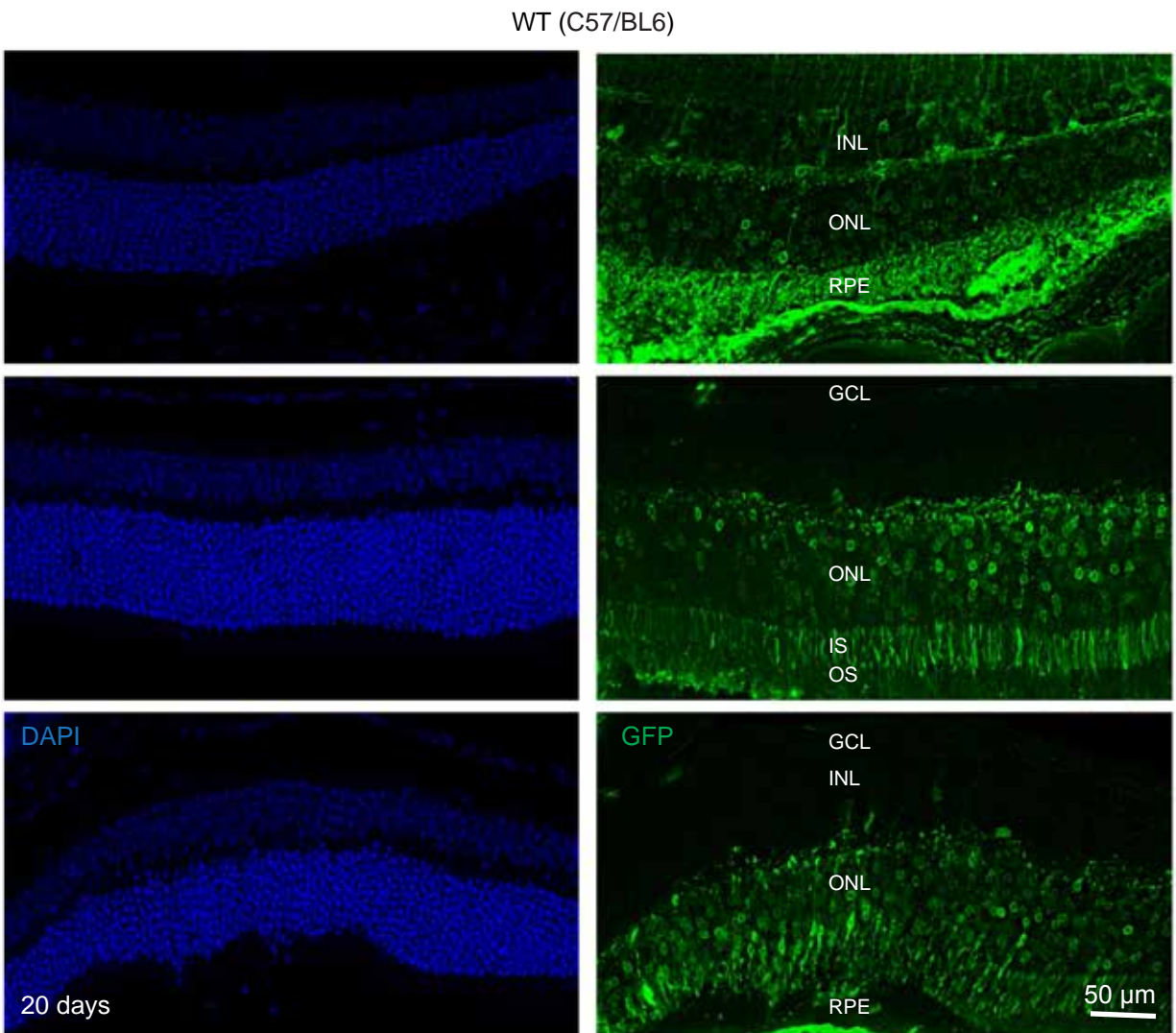


Figure S13. Transduction of mouse retina with AAV9-PHP.B-CBA-GFP. Adult (4.5 months) C57/BL6 mice were injected subretinally with AAV9-PHP.B-CBA-GFP (2.1×10^9 vg contained in 1μ l). (A) Many retinal cells were transduced after 20 days post injection. (B) Numerous photoreceptors were GFP-positive GCL: ganglion cell layer, INL: inner nuclear layer; ONL: outer nuclear layer; RPE, retinal pigment epithelium.

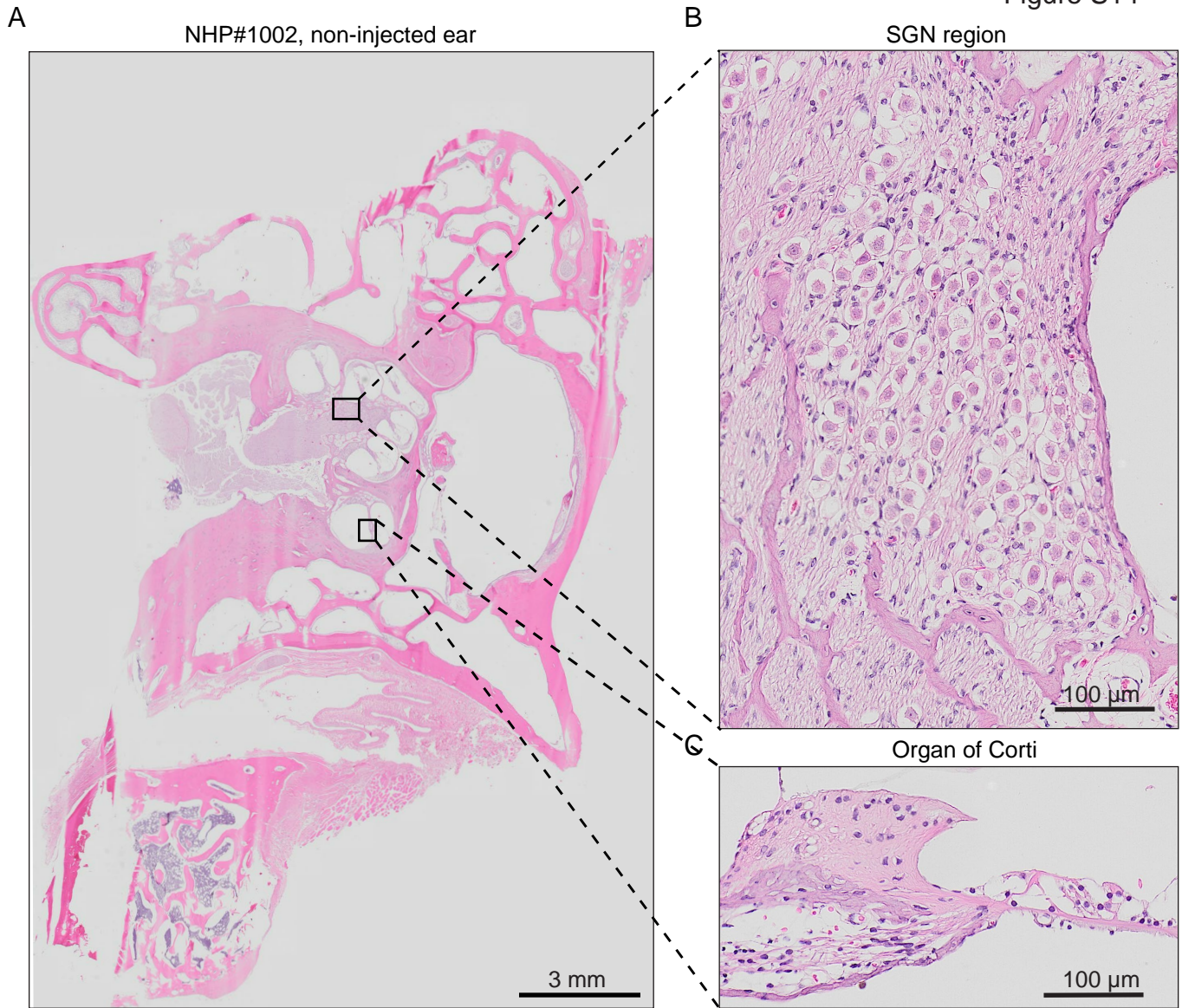


Figure S14. Hematoxylin and Eosin staining of the non-injected ear of Cynomolgus monkey #1002. (A) A low magnification image is shown with areas of interest indicated by rectangles. Magnified image of spiral ganglion neurons (SGN) region (B) and organ of Corti (C).

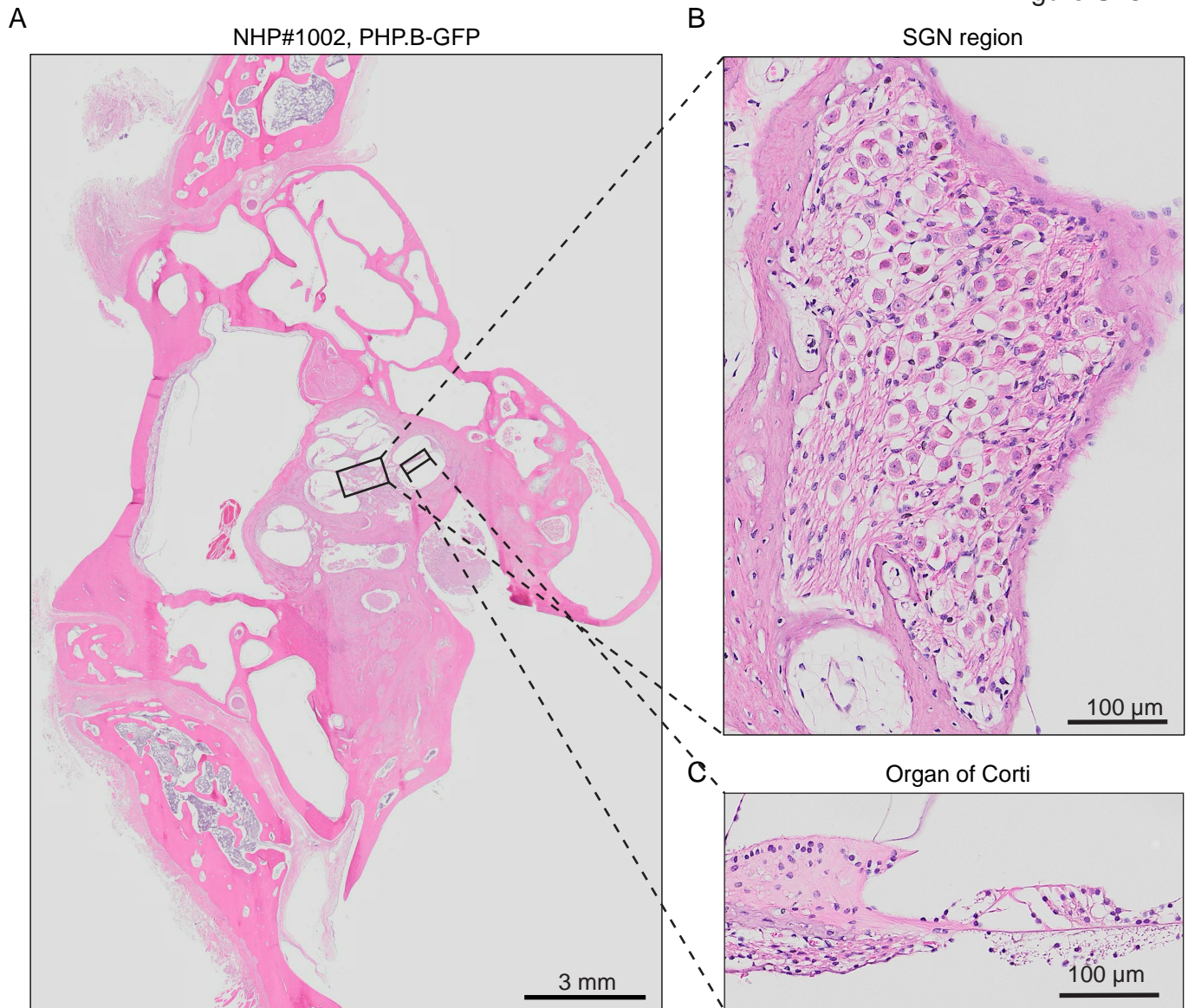


Figure S15. Hematoxylin and Eosin staining of the AAV9-PHP.B-CBA-GFP (3×10^{11} VG) injected ear of Cynomolgus monkey #1002. (A) A low magnification image is shown with areas of interest indicated by rectangles. Magnified image of spiral ganglion neurons (SGN) region (B) and organ of Corti (C) show normal cellular morphology.

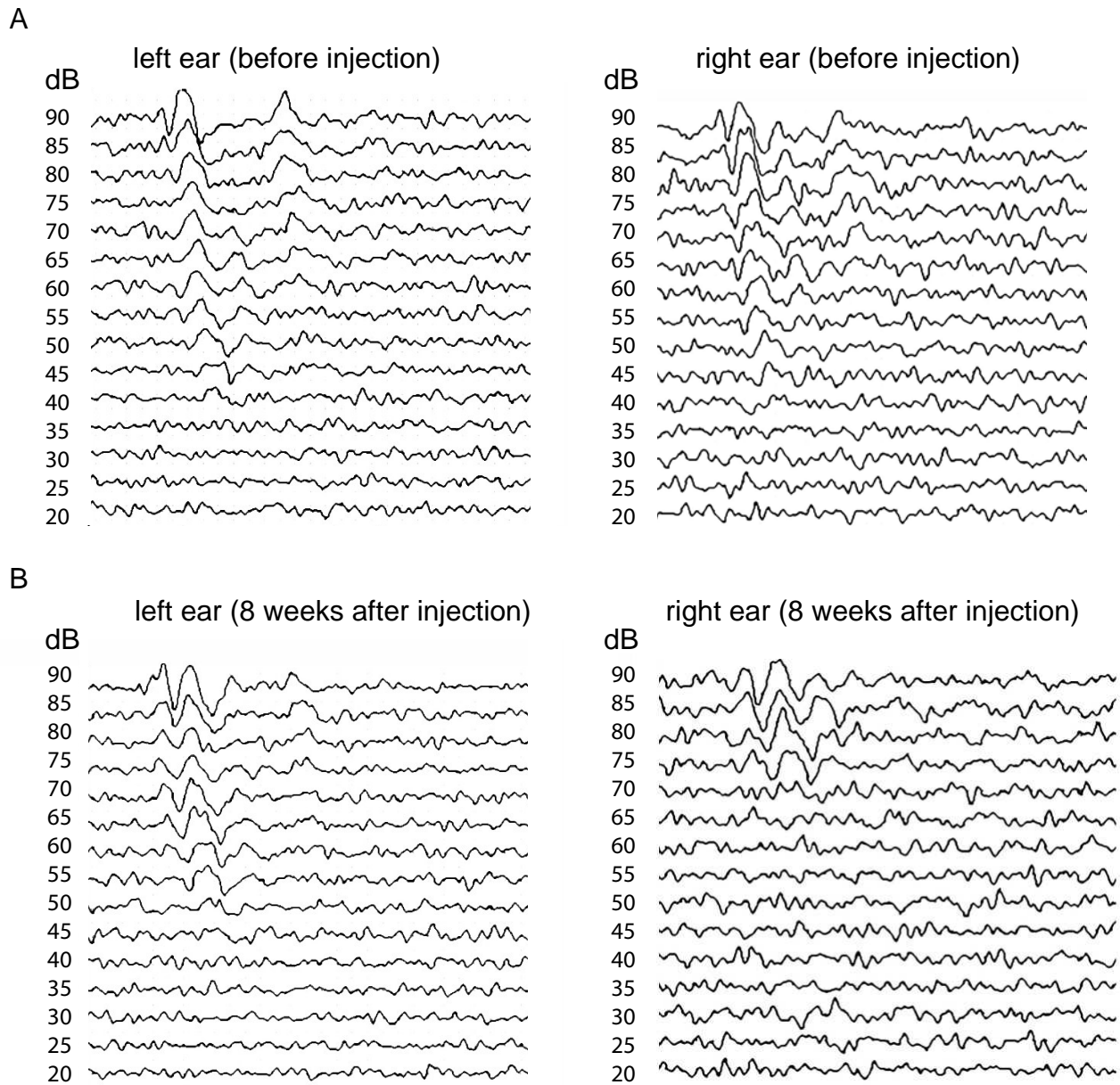


Figure S16. ABR test of Cynomolgus monkey #3501 injected with AAV9-PHP.B-CBA-GFP (1×10^{11} VG) before (A) and 8 weeks after injection (B).

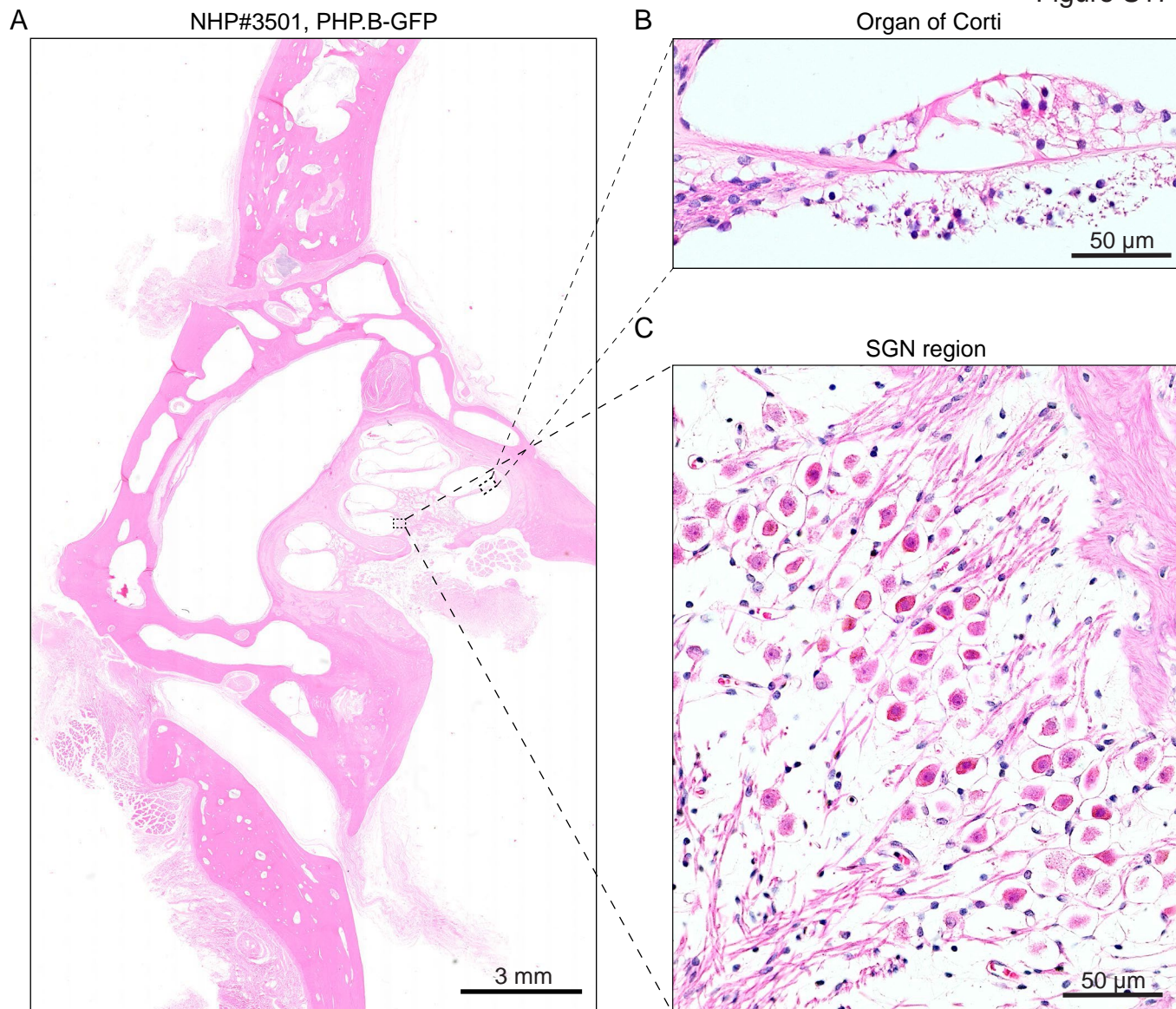


Figure S17. Hematoxylin and Eosin staining of the AAV9-PHP.B-CBA-GFP (1×10^{11} VG) left injected ear of Cynomolgus monkey #3501. (A) A low magnification image is shown with areas of interest indicated by rectangles. (B) Magnified image of organ of Corti and (C) spiral ganglion neurons (SGN) region.

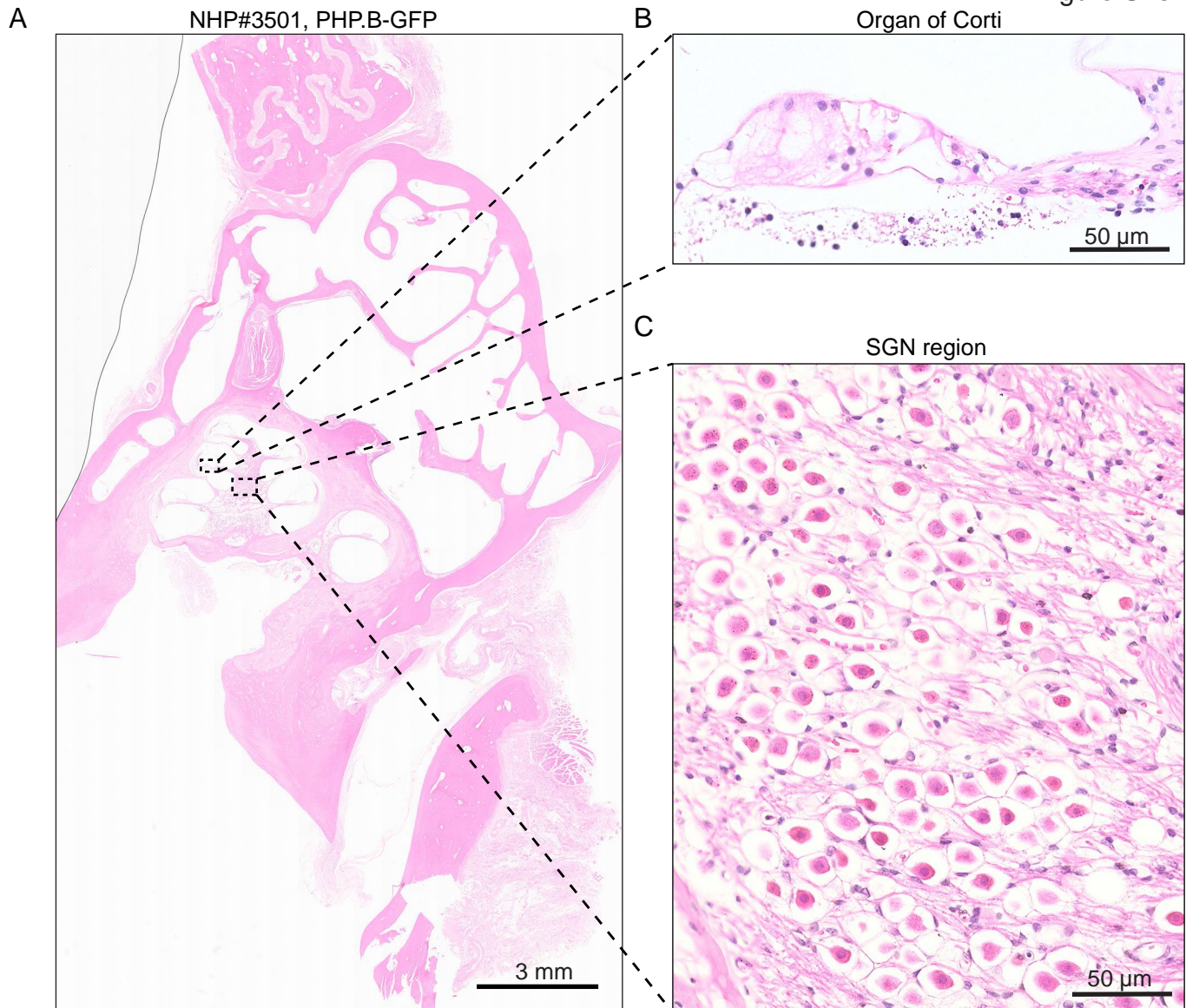


Figure S18 Hematoxylin and Eosin staining of the AAV9-PHP.B-CBA-GFP (1×10^{11} VG) right injected ear of Cynomolgus monkey #3501. (A) A low magnification image is shown with areas of interest indicated by rectangles. (B) Magnified image of organ of Corti and (C) spiral ganglion neurons (SGN) region .

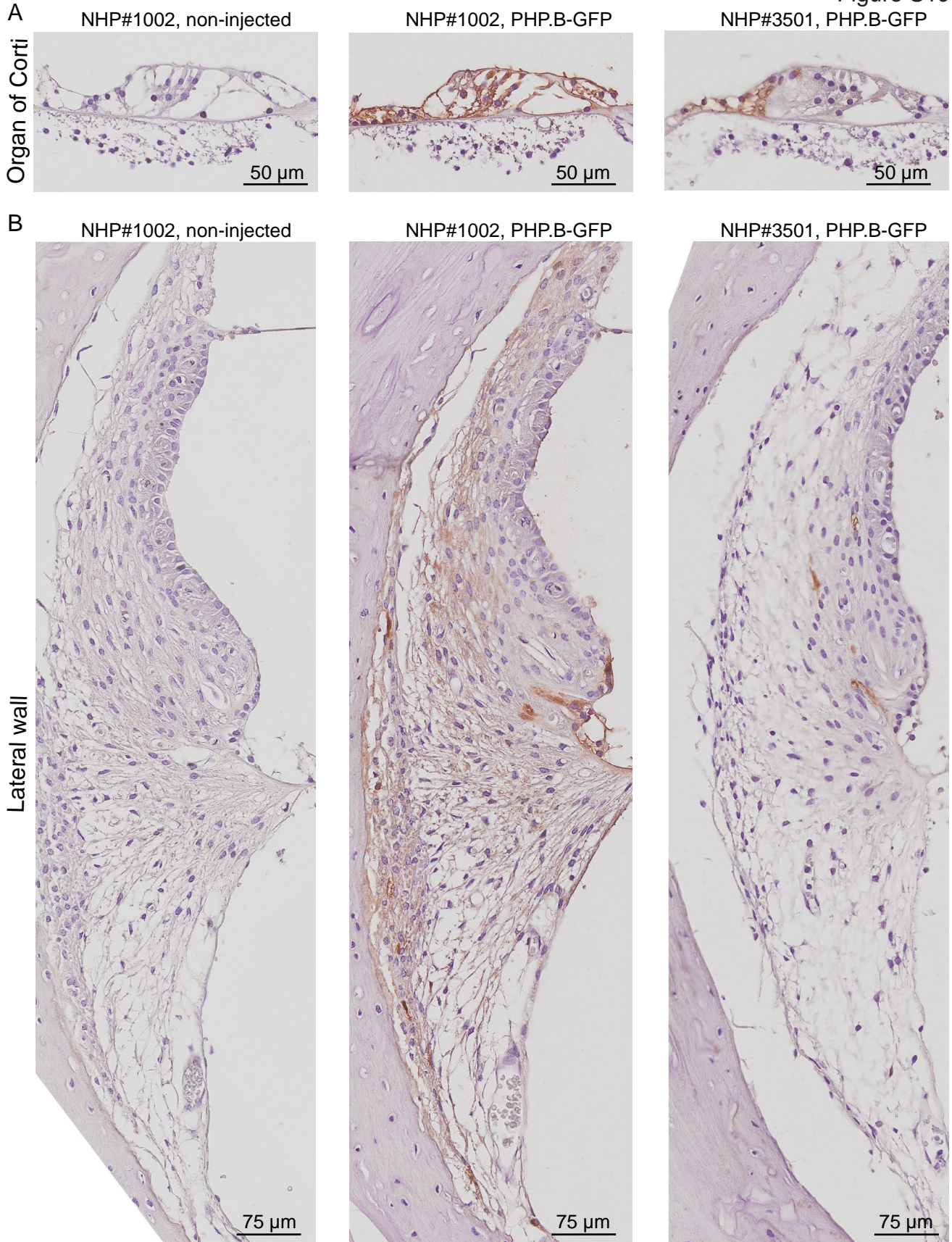


Figure S19. Transduction profile of AAV9-PHP.B-CBA-GFP in the organ of Corti and lateral wall of Cynomolgus monkeys #1002, injected with AAV9-PHP.B-CBA-GFP (3×10^{11} VG) and #3501, injected with AAV9-PHP.B-CBA-GFP (1×10^{11} VG). **(A)** Organ of Corti of non-injected ear (left) and injected ear (middle) of Cynomolgus monkey #1002 and injected ear (right) of Cynomolgus monkey #3501. **(B)** The lateral wall of non-injected ear (left) and injected ear (middle) of Cynomolgus monkey #1002 and injected ear (right) of Cynomolgus monkey #3501.